THE EFFECTS OF THE STEREOCHEMISTRY OF RUTHENIUM (II) POLYPYRIDYL COMPLEXES ON MICROTUBULES AS TARGETS FOR CHEMOTHERAPY

by

RADHIYAH HIMAWAN

Presented to the Faculty of the Graduate School of

The University of Texas at Arlington

Of the Requirements for the Degree of

MASTER OF SCIENCE IN CHEMISTRY

THE UNIVERSITY OF TEXAS AT ARLINGTON

MAY 2019

ACKNOWLEDGEMENTS

I would like to express the greatest thanks to Dr. Frederick MacDonnell for giving me this opportunity to study under him. Without him I would've never known how much I loved research. His mentorship helped me grow as a researcher. Special thanks to Dr. Nagham Alatrash and Dr. Cynthia Griffith for all their hard work in teaching me the ropes of not only research, but also about what it takes to be a woman in science. Nagham and Cynthia were vital in the preliminary biological and synthesis work. I would like to highlight that Nagham provided a vast database of cell free and cell assay work as well as being the first person in the lab to successfully resolve the RPCs, and Cynthia provided me with all the chiral HPLC data. They also taught me how to run countless numbers of instruments and tests for which I can't thank them enough. I wouldn't be where I am without them today and I couldn't have asked for better mentors.

I would like to thank Dr. Faiza Issa for teaching me how to run the biological assays and how to troubleshoot them. I would like to express thanks to Dr. Delphine Gout for the crystal structures and helping me initially realize that some of my resolving salts had racemized and weren't what I thought they were, leading me to be able to successfully optimize their synthesis. I would like to thank C. Philip Shelor for the ruthenium analysis via ICP-MS.

I would like to thank the University of Texas at Arlington, the Shimadzu Center, and the Welch Foundation for providing the facility, the materials, and funding.

Biggest thanks to all my fellow graduate students, especially Abiud Portillo, Adway Zacharias, Shariq Haseen, Melissa Reardon, Thalia Garcia, Yu-Sheng (Sam) Sung, and Elizabeth (Beth) Readel, for always being there to struggle with me. I couldn't have done it without your support system.

I would like to express my appreciation to the undergraduates of the lab, Asiah Himawan, Christian Torres, and Matthew Guerrero for helping me with starting material, buffers, and maintaining the glassware, as well as their company when I would have otherwise had to work alone.

I would like to especially thank my family: my sister Asiah for her support in the lab and as a fantastic sister; my moms, Edvarina Edwar and Ignacia Barrios, for always ensuring my health, keeping me fed, finding the best ways to help me de-stress, and being the greatest cheerleaders; the dads, the rest of my friends, my best friend, Dimple Raval, extended family, and the Malindo community for all their support.

Finally, to my better half, Alejandro Diaz Barrios, a great many thanks for the patience, time spent with me in lab at ungodly hours, helping me with my course work, all the cooking, cleaning, and shopping on days I simply couldn't function. I was given everything a woman could ask for and more, and this support was essential to the completion of this thesis.

ABSTRACT

THE EFFECTS OF THE STEREOCHEMISTRY OF RUTHENIUM (II) POLYPYRIDYL COMPLEXES ON MICROTUBULES AS TARGETS FOR CHEMOTHERAPY

Radhiyah Himawan, M.S.

The University of Texas at Arlington, 2019

Supervising Professor: Frederick M. MacDonnell

Ruthenium polypyridyl complexes (RPCs) are promising anticancer agents due to their robustness and tunability of their polypyridyl ligands. Their axial chirality generally allows for more selective binding to biological molecules. The ruthenium complexes $[Ru(phen)_3]Cl_2$ (RPC **1**), $[Ru(DIP)_3]Cl_2$ (RPC **2**), $[(phen)_2Ru(tatpp)]Cl_2$ (RPC **3**), $[(phen)_2Ru(tatpp)Ru(phen)_2]Cl_4$ (RPC **4**), and $[(phen)_2Ru(dppz)]Cl_2$ (RPC **5**) have all been investigated, and RPCs **2**, **3**, and **4** have shown lower micromolar cytotoxicity against malignant cell lines without irradiation. Herein we show that microtubules (MTs) may be the target of some RPCs in cells and all these RPCs **1-5** promote tubulin polymerization *in vitro*. How they interact with MTs is still yet to be discovered.

We examined how the different enantiomers of RPC **2** and **3** affected the cytotoxicity, the cellular uptake, and the MT polymerization. Chapter 1 of this thesis reviews prior literature and discusses other metal complexes as well as RPCs that have anticancer potential for their cellular target and correlation to their structures. Chapters 2 and 3 presents how the stereochemistry of the RPCs in their chloride salt affects their ability to stabilize MTs in addition to entering the cell in the first place. Chapter 2 also presents evidence that MT stabilization by RPCs may not be

simple due to electrostatic interactions. MT stabilization is done by comparing the *in vitro* polymerization of free tubulin with and without the presence of the microtubule stabilizing agent (MSA) as a factor of increased light scattering at 340 nm. Cellular uptake is done in the non-small cell lung carcinoma cell line, H358. The amount of ruthenium was analyzed using ICP-MS and the protein concentration using a bicinchoninic acid assay and UV-Vis spectrometry. Although there were no significant chiral differences in MT stabilization, there was a difference in cellular uptake of enantiopure RPC **2**. Chapter 4 outlines the resolution of the RPCs by use of $Na_2[As_2$(+ or -)$tartrate_2]$ and $Na_2[Sb_2$(+ or -)$tartrate_2]$, as well discussing the optimization of the syntheses of $Na_2[Sb_2$(+ or -)$tartrate_2]$ and $K_2[Sb_2$(+ or -)$tartrate_2]$.

TABLE OF CONTENTS

LIST OF ILLUSTRATIONS

LIST OF SCHEMES

LIST OF TABLES

LIST OF ABBREVIATIONS

ACE	Acetylcholinesterase
Bpy	2,2’-bipyridine
BSA	Bovine serum albumin
CppH	2-pyridyl-2-pyrimidine-4-carboxylic acid
CD	Circular dichroism
DIP	4,7-diphenyl-1,10-phenanthroline
DNA	Deoxyribonucleic acid
Dppz	Dipyrido[3,2-a:2’,3’-c]phenazine
DSB	Double-strand DNA breakage
DSC	Differential scanning calorimetry
GTP	Guanosine-5'-triphosphate
HPLC	High performance liquid chromatography
IP	Interperitoneally
ITC	Isothermal calorimetry
MDA	Microtubule destabilizing agent
MT	Microtubule
MSA	Microtubule stabilizing agent
NSCLC	Non-small cell lung carcinoma
H358	Human non-small cell lung carcinoma
HeLa	Human cervical cancer

IC_{50}	Inhibitory concentration 50
ICP-MS	Inductively coupled plasma mass spectrometry
PARP	Poly-ADP ribose polymerase
Phen	1,10-phenanthroline
Phendione	1,10-phenanthroline-5,6-dione
ROS	Reactive oxygen specie
RPC	Ruthenium polypyridyl complex
Tatpp	9,11,20,22-tetraazatetrapyrido[3,2-a:2’,3’-c:3’‘,2’‘-l:2’“,3’“-n]pentacene

CHAPTER 1. CELLULAR TARGETS AND ACTION OF RUTHENIUM CYTOTOXIC AGENTS

1.1 Ruthenium Polypyridyl Complex Family

Ruthenium polypyridyl complexes (RPCs) comprise of a broad class of compounds in which ruthenium (II) is coordinated to at least one polypyridine ligand, such as 2,2'-bipyridine (bpy), 1,10-phenanthroline (phen), and 4,7-diphenyl-1,10-phenanthroline (DIP) shown in Figure 1.1. When these complexes are coordinatively saturated with polypyridine ligands, i.e. $[Ru(N\text{-}N)_3]^{2+}$ or $[Ru(N\text{-}N\text{-}N)_2]^{2+}$, they are exceptionally robust and kinetically inert, such that they can survive *in vivo* without being metabolized in many cases. In addition to homoleptic complexes, a variety of heteroleptic RPCs may be prepared and investigated. For the purpose of this thesis, the RPCs will be limited to those that are coordinatively saturated with polypyridyl ligands. Other important ligands include dipyrido[3,2-a:2',3'-c]phenazine (dppz), 1,10-phenanthroline-5,6-dione (phendione), and 9,11,20,22-tetraazatetrapyrido[3,2-a:2',3'-c:3'',2''-l:2''',3'''-n]pentacene (tatpp). These aromatic ligands are multidentate and have strong π backbonding that allow for greater electron mobility throughout the complex. As a result, these complexes are more stable and are often luminescent with highly tunable electron transfers.[1]

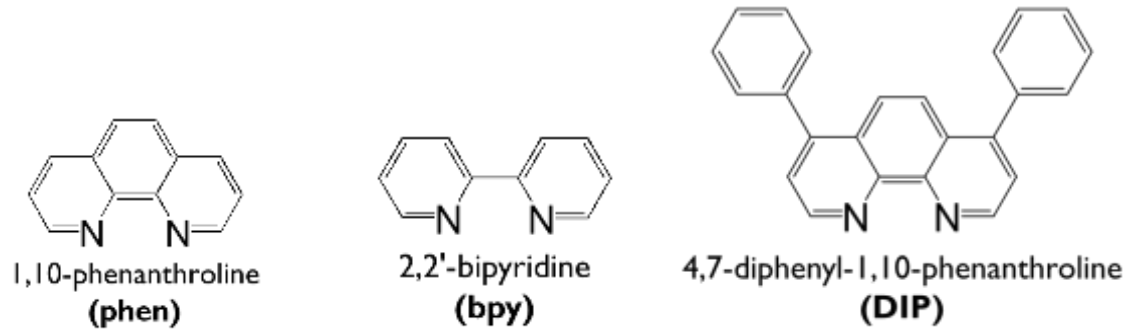

Figure 1.1: The chemical structures of some polypyridyl ligands.

1.2 RPCs in Biological Systems

Due to their robustness and tunability, RPCs have been used in biological systems for many years. The simplest of them, $[Ru(phen)_3]Cl_2$, have been used for markers in the sheep digestive tract as they were not appreciable absorbed into the intestinal tract and were fully excreted, unmetabolized, in the urine and feces.[2] RPCs have also been found to have bacteriostatic activity as well as having been studied to interact and alter DNA and enzymes.[3-5]

Since RPCs are positively charged, it can be argued that it would interact electrostatically with the negatively charged DNA phosphate backbone. However, electrostatic interactions alone do not explain the chiral preference for the unwinding of supercoiled pColE1 plasmid DNA observed by Barton. It was observed that only 90 μM of the Δ enantiomer was needed to fully unwind negatively supercoiled DNA, while 120 μM of the Λ enantiomer was needed. She determined that the unwinding angle of $[Ru(phen)_3]^{2+}$ was the same as that of ethidium bromide, suggesting an intercalative interaction. She then confirmed that the π cloud of one of the phen ligands intercalated in the major groove of B-DNA, which would explain the preference for the Δ enantiomer with B-DNA, since they are both right-handed helices.[5]

Dwyer *et al.* also noticed that there was a chiral difference in the animal toxicity of simple tris homoleptic RPC. However, it is the reverse what is expected: the Δ enantiomer of $[Ru(phen)_3](ClO_4)_2$ has a lethal dose of 18.4 $mg \cdot kg^{-1}$ while the Λ has a lethal dose of 9.2 $mg \cdot kg^{-1}$ delivered interperitoneally (IP). The $[Ru(bpy)_3](ClO_4)_2$ has a similar trend but the difference less staggering with the Δ enantiomer having a lethal dose of 16.8 $mg \cdot kg^{-1}$ and the Λ having a lethal dose of 15.7 $mg \cdot kg^{-1}$. They attributed animal toxicity to inhibition of acetylcholinesterase (ACE). When the

enzyme and substrate were isolated and treated with enantiopure RPCs, they noticed a 90% inhibition by the Λ enantiomer at 10^{-4} M while the Δ enantiomer only showed 20% inhibition.[5] The anionic active site of ACE has two glutamate residues as well as an aromatic tryptophan residue that would interact with the dicationic and aromatic RPC, with the Λ interacting best with the L-amino acids.[6, 7]

1.3 Cellular Targets of Cytotoxic Metal Agents

The manner by which simple inorganic drugs interact with cellular structures is still an open question in many cases. Platinum-based antineoplastic agents, including the tremendously successful anticancer drug cisplatin, *cis*-$Pt(NH_3)_2Cl_2$, and its derivatives of carboplatin, and oxaliplatin, are shown to target nuclear DNA, as well as cysteines in numerous proteins. They do this by exchanging the labile chloride ligands with water which can then covalently bind to guanine nucleotides and cysteine residues.[8, 9] In fact, ruthenium (III) complexes, such as NAMI-A and KP1019, and ruthenium (II) arene complexes are proposed to attack DNA and kinases in much the same way.[9-12] Gold and titanoene complexes target specific proteins or DNA, as indicated in Table 1.1.[9] RPCs are implicated as attacking multiple targets, including the nuclear DNA, mitochondria, cell membrane, and membrane proteins, which suggests that small variations in RPC structure may induce different cellular targets and modes of action.[8-20] A suggested interaction is through generation of reactive oxygen species (ROS) through redox reactions with molecules in the cells such as glutathione (GSH), which can cause an imbalance in the mitochondrial membrane potential that results in apoptosis.[8, 13] Figure 1.2 shows the structures of some reported RPCs with low micromolar cytotoxicity.

Despite the similarities in their structures, their functions are completely different. RPC **1** is the simplest of the complexes shown and has a moderate IC_{50} of 86.7 ± 4.1 μM against the H358, human non-small cell lung carcinoma (NSCLC), cell line.[6] Barton had observed the complex to the intercalate isolated DNA,[4] however, experimentation in the MacDonnell lab has shown that the hydrophilicity of the complex inhibits it from passing through cell membrane, much less the nuclear envelope.[6] Hence, this might explain the increased IC_{50} compared to all the other complexes. Structurally, RPC 5 is the most similar to RPC **1** and it has the second highest IC_{50} of 35 ± 0.71 μM to match.[6] It intercalates DNA similarly to RPC **1**, but the dppz ligand creates a better π interaction than the phen of RPC 1 and the luminescence that appears from the charge transfer can explain its slightly lower IC_{50} value.[14] Neither RPC **1** nor RPC **5** actually cleave DNA, but they disrupt the DNA structure to result in cytotoxicity.[13] RPC **3** and RPC **4** were found to be selectively cytotoxic against malignant cell lines, while RPC **2** was cytotoxic against all cell lines tested, even more so than cisplatin in most cell lines, with an IC_{50} of 1.7 ± 2.3 μM against H358.[6,15] The cytotoxicity of RPC **2** is partly due to its lipophilicity, allowing for easy transport into the cell.[6] Once it enters the cell, it has been observed to remain in the cytoplasm and accumulates in the mitochondria and lysosome, activating poly-ADP ribose polymerase (PARP) cleavage and caspase induced apoptosis when exposed to light.[16] *In vitro* cell-free assays, RPC **2** has been shown by Goldstein *et al*. to intercalate DNA, however, much like RPC **1** and RPC **5**, it does not cleave cellular DNA.[13, 17] RPC **3** and RPC **4**, on the other hand, has been shown to be actively transported into the cell and observed to cause double-strand DNA breakages (DSB) through ROS generation in the presence of glutathione (GSH).[13, 15] The selectivity could be explained by the upregulation of

GSH in malignant cell lines.[18] Against H358, RPC **3** and **4** have IC_{50}'s of 13.2 ± 1.8 μM and 15.2 ± 1.8 μM, respectively.[6]

Table 1.1. Cellular Targets of Known Cytotoxic Metal Agents

Drug	**Metal**	**Proposed Cellular Target**	**Location**	**Ref.**
Platin Family	Pt (IV)	DNA	Nucleus	9
Picoplatin	Pt (IV)	DNA, GSH, cysteine	Nucleus, cytoplasm	9
BBR3464	Pt (II)	DNA (long-range cross linking)	Nucleus	9
NAMI-A	Ru (III)	DNA	Nucleus	9, 10
KP1019	Ru (III)	DNA	Nucleus	9, 11
RPC	Ru (II)	Mitochondria (ROS generation, membrane depolarization)	Mitochondria	9
Ruthenium Arene Complexes	Ru (II)	DNA, kinase	Nucleus, cytoplasm	9, 12
Gold Imidazoles	Au (I), (III)	Zinc finger	Nucleus	9
Gold Carbenes	Au (III)	GSH, cysteine	Cytoplasm	9
Gold Dithiocarbamates	Au (III)	Protease, deubiquitinase	Cytoplasm	9
Titanocene	Ti (IV)	DNA	Nucleus	9

DNA: deoxyribonucleic acid; GSH: glutathione; ROS: reactive oxygen species

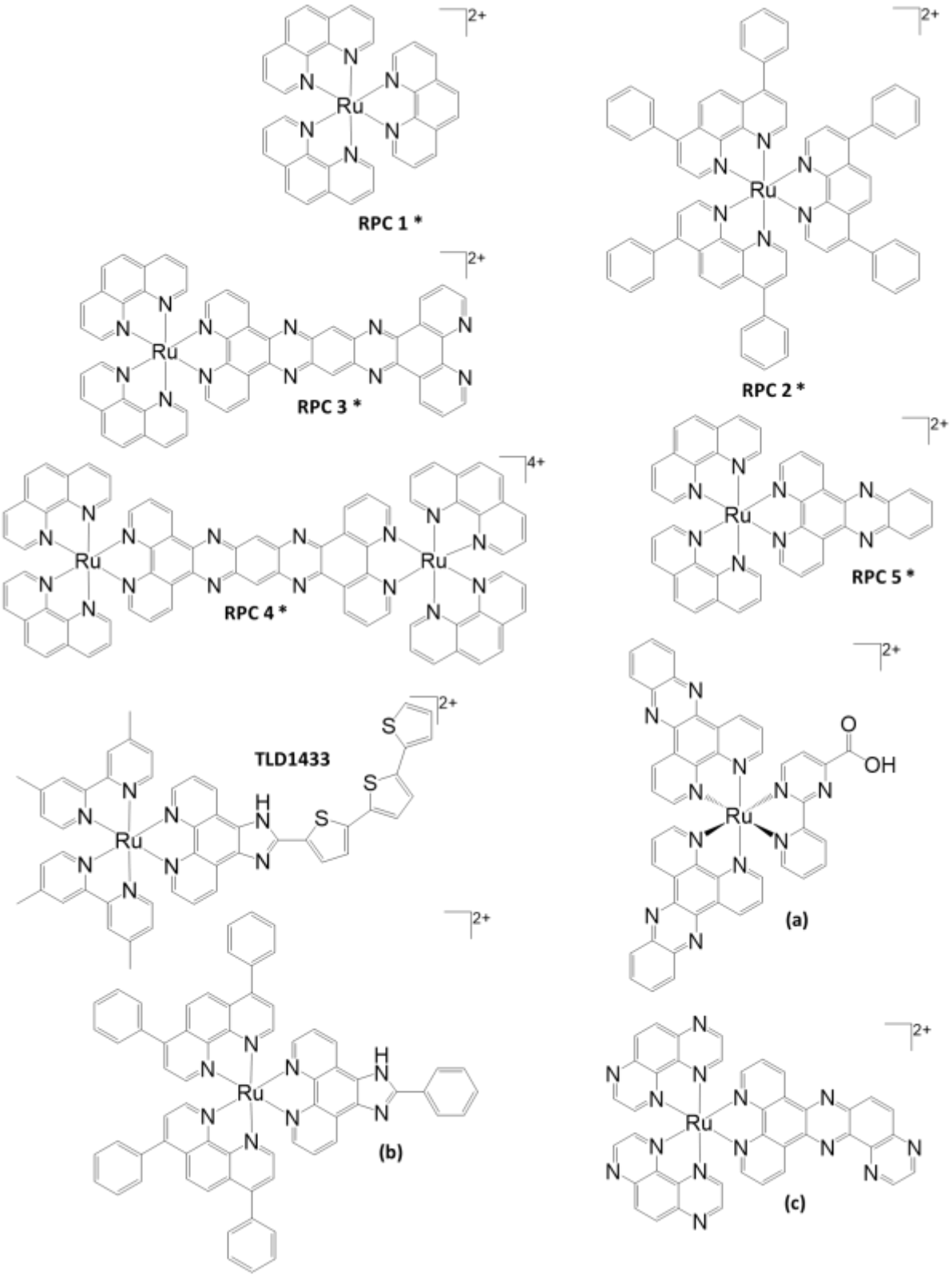

*Under study in this work.

Figure 1.2: The chemical structures of reported RPCs.

Complex **(c)** is most similar to RPC **5** but instead of interrupting DNA, it accumulates in the mitochondria and lysosome around the nucleus and induce cell apoptosis through ROS generation. Before irradiation, its IC_{50} ranges from >100 to 40.2 μM, but when irradiated it ranges from 42.8 to 8.8 μM.[19] This suggests that irradiation generates an excite state that produces ROS and it is likely that the additional nitrogens allow for this excited state that does not exist in RPC **5**. However, the advantages to this is limited because irradiation could be difficult to do in spheroid cell growths that are more similar to actual tumors. Complex **(a)** has two dppz ligands and one 2-pyridyl-2-pyrimidine-4-carboxylic acid (CppH), but its target is also the mitochondria and not DNA like RPC **5**. In fact, complex **(a)** hardly accumulates in the nucleus at all and actually localizes in the cytoplasm. Unlike complex **(c)**, complex **(a)** does not require radiation and has a significantly low IC_{50} of 10.0 ± 1.3 against HeLa cell lines. Structurally, this could be because the dppz ligands better shield the positive ruthenium core and increases its hydrophobicity relative to complex **(c)** despite its carboxylic acid group.[20] Complex **(b)** appears very similar to RPC **2** but without irradiation, it hardly affects the cell, and even with irradiation, only had an IC_{50} range of 15.5 to 12.4 μM.[19] The underlying reason for the cytotoxicity of RPC **2** lies in its hydrophobicity.[6] Replacing the DIP ligand with the imidazole derivative would increase the hydrophilicity, sacrificing cytotoxicity, but it could help decrease animal toxicity by making it more selective since it can pass harmlessly through the animal in the dark. TLD1433 is also an imidazole derivative of the 3,4,7,8-tetramethyl-1,10-phenanthroline that ends in a chain of thiophenes. The complex is relatively nonfunctioning under hypoxia conditions of human tumors, but the cyclometalated versions have achieved better success as a photodynamic therapy agent.[19, 21]

Chemotherapeutic agents, whether used in the dark or irradiated, have to be able to function under the less than ideal tumor conditions with decreased nutrient intake and hypoxia due to the decreased surface area. In order for the drugs to disrupt function in its target organelle, it must first accumulate at the site. RPC **1** has shown to barely get taken into the cell at all, which might explain the lack of activity in cells despite having activity *in vitro*.[15] This raises the question if even enough of the RPCs even accumulate in the proposed target organelles to result in their observed cytotoxicity.

1.4 Scope of Thesis

RPCs seem to have increased interaction with chiral biological molecules, and since most biological molecules are chiral, such as right-handed B-DNA and enzyme active sites made with L-amino acids, an increased interaction is expected with the matching RPC handedness. It is postulated that determining the drug interaction site with the RPC could help with understanding the cause of cytotoxicity and how to alter the complex to make the complex more selectively cytotoxic as well as help it overcome any limitations in the less than ideal conditions of a human tumor.

CHAPTER 2. EXPLORING THE EFFECT OF RPCS ON MT STABILIZATION IN VITRO

2.1 Introduction

Recent work in the MacDonnell lab reveals that RPC **2** and possibly other RPCs function via a direct interaction with the cellular microtubules (MT) in a manner which disrupts normal dynamic tubulin polymerization and depolymerization. To the best of our knowledge, this is the only small molecule metal complex ever shown to alter MT dynamics in cells and suggests that RPCs, through proper structural modifications, could be evolved into potent drugs for disruption of MT function. The first indication that MTs were being targeted was the elevated concentration of the RPCs found in this particular cellular component. Cultured human H358 cells treated with 20 μM of RPC **2** for 12 hours were fractionated into four components: cytosol, nucleus, golgi-mitochondria-membrane proteins, and the cytoskeleton, which were then examined for ruthenium content by induced coupled plasma mass spectrometry (ICP-MS). Over 95% of ruthenium absorbed by the cell was found in the cytoskeletal fraction. The concentration of the drug in this one fraction suggested a specific and reasonably tight binding to the proteins in it, which consists principally of tubulin and microtubules, actin, and intermediate filaments. The cytoskeleton as a target is further supported by observations made by Alatrash in the MacDonnell group. Her differential confocal image shows striations in between MCF7 cells that have been treated with RPC **2**, indicating attenuation of cytokinesis.

The cellular cytoskeleton is an attractive target for many antineoplastic drugs as disruption of normal MT function, for example, can lead to failed mitosis and cell death. Taxanes are clinically used microtubule stabilizing agents (MSAs), while vincristine, colchicine, and

nocodazole are clinically used microtubule destabilizing agents (MDAs). Taxanes have a known binding site on the β-subunit of the tubulin heterodimer and most MDAs bind at a discrete site at the α/β dimer interface.[22-24] An in vitro examination of the effect of RPC **2** on tubulin polymerization, using purified tubulin in the presence of guanosine-5'-triphosphate (GTP), reveals it to act as a MSA. In this experiment, a temperature jump, from 4°C to 37°C, initiates the normal porcine tubulin polymerization reaction, which is monitored by measuring the increasing turbidity of the solution as the MTs form.[25] Addition of RPC **2** shows an acceleration of the polymerization reaction and a greater degree of polymerization at steady state than the untreated control at a level comparable to docetaxel. Notably, the normal lag phase seen before rapid polymerization for the control is absent when Taxol is present. RPC **2**, which otherwise mimics Taxol, shows a lag phase similar in duration to the control, indicating some important differences. Interestingly, all RPCs examined, **1**–**5**, caused MSA activity in the polymerization assay, albeit to different degrees. It was also determined that the concentration of dimethyl sulfoxide (DMSO) used to dilute the drug as well as the resulting colors of the drugs were insignificant to the absorbance. It is possible that this stabilization is observed due to the di-cation effect.[26, 27] This is unlikely since other experiments have suggested that this stabilization also occurs in cells, but in order to rule out the di-cation effect, an assay with other general di-cations, Mg^{2+} and Ca^{2+} will also be ran.

In the present studies, we examined how enantiopure mononuclear RPCs behaved compared to their enantiomer and the racemate. In these next chapters, we examined the effects of chirality of the polymerization kinetics, cellular uptake for RPC **2**, and cytotoxicity. Due to the

extremely small amount of RPC **1** that enters the cell, the effects of its chirality on MT stabilization will not be tested in this study.

2.2 Experimental Section

2.2.1 Chemicals

The lyophilized tubulin protein, GTP, and buffers for this experiment—piperazine-N,N'-bis[2-ethanesulfonic acid] sequisodium (PIPES), magnesium chloride, ethylene glycol-bis(b-amino-ethyl ether) N,N,N',N'-tetra-acetic acid (EGTA), and glycerol—were obtained from the Cytoskeleton, Inc. (Denver, CO) Tubulin Polymerization Assay Kit (Cat: BK006P) and used as directed. The 1x general tubulin buffer was reconstituted to 10 mL using autoclaved Millipore water. The GTP was reconstituted with 100 µL of autoclaved Millipore water to make 100 µM stock solutions that were then aliquoted into 10 µL tubes which were stored at -80°C. 10 µL of 100 µM stock solution was added to 1.1 mL of reconstituted general buffer that was kept on ice. The 1.1 mL of this supplemented buffer was used to reconstitute the tubulin protein to make 10mg/mL tubulin that were aliquoted into 200 µL cryotubes which were immediately dropped into a dewar filled with liquid nitrogen before storing at -80°C. All reagents and solvents were reagent grade and used as is unless specified. Enantiopure RPCs were isolated by resolution of the racemic starting materials with either sodium arsenyl (+ or -) tartrate or sodium antimonyl (+ or -) tartrate as described in the last chapter, except for Δ- and Λ-RPC **3** which were prepared by stereospecific derivations of their known syntheses.[28, 29] RPCs **2**-**5** in their chloride salts were dissolved in DMSO from Sigma-Aldrich. The racemic salts were dissolved as is and the enantiomers were resolved using a method modified from the one derived by Sun *et al.* as

described later.[28] Stock solutions of 2 mM of $MgCl_2$, and $CaCl_2$ were prepared in sterile Millipore water.

2.2.2 Instrumentation

The spectrophotometer used was the BGM LABTECH FLUOstar Omega. A Costar 96-Well Half-Area plate was used. The settings were: positioning delay: 0.4; No. kinetic window: 1; No. of cycles: 61; Measurement start time: 0.0; No off flashes per well and cycle: 20; Cycle time: 60; wavelength: 340; Pathlength correction: on; Volume: 110.0; Length: 6.91; No pauses between cycles; Reading direction from left to right with no replicates.

2.2.3 Experimental Procedure

The 96-well plate was warmed at 37°C in an incubator for thirty minutes and the oven in the spectrophotometer was warmed to 37°C. The plate was then removed from the incubator. The first well was the blank, which had 110 µL of room temperature general buffer. Three control wells had 10 µL of room temperature general buffer added to them. The 2 mM stock solutions of racemic RPC **2** in DMSO was diluted to 0.1 mM using general buffer and 10 µL of this was added to three wells at room temperature. The 2 mM stock solutions of Δ- and Λ-RPC **2** were diluted and added to the plate in a similar manner. The plate was then incubated at 37°C degrees for two minutes. The cold (4°C) polymerization buffer containing 80 mM of PIPES at pH 6.9, 2 mM of $MgCl_2$, 0.5 mM EGTA, 10.2% glycerol, and 1 mM GTP was made and used to dilute the cold reconstituted tubulin to 3 mg/mL tubulin which was kept on ice. From this diluted tubulin, 100 µL was then added to the warmed control and drugs on the plate. The plate was then placed into

the spectrophotometer and the absorbance at 340 nm was recorded every minute for 61 minutes. The resulting graphs were then obtained from the computer and manipulated.

The general di-cations, $MgCl_2$ and $CaCl_2$, and other RPCs **3** and **5** were tested in a similar manner. In order to normalize the plots and allow for comparisons, the rate of rapid polymerization of the controls were corrected to have a rate of 17 OD/min as assigned in the Cytoskeleton manual, and the max absorbance was normalized to 0.350 OD.

2.3 Results and Discussion

The effect of the presence of a general di-cation on the polymerization of free tubulin can be seen in Figure 2.1.

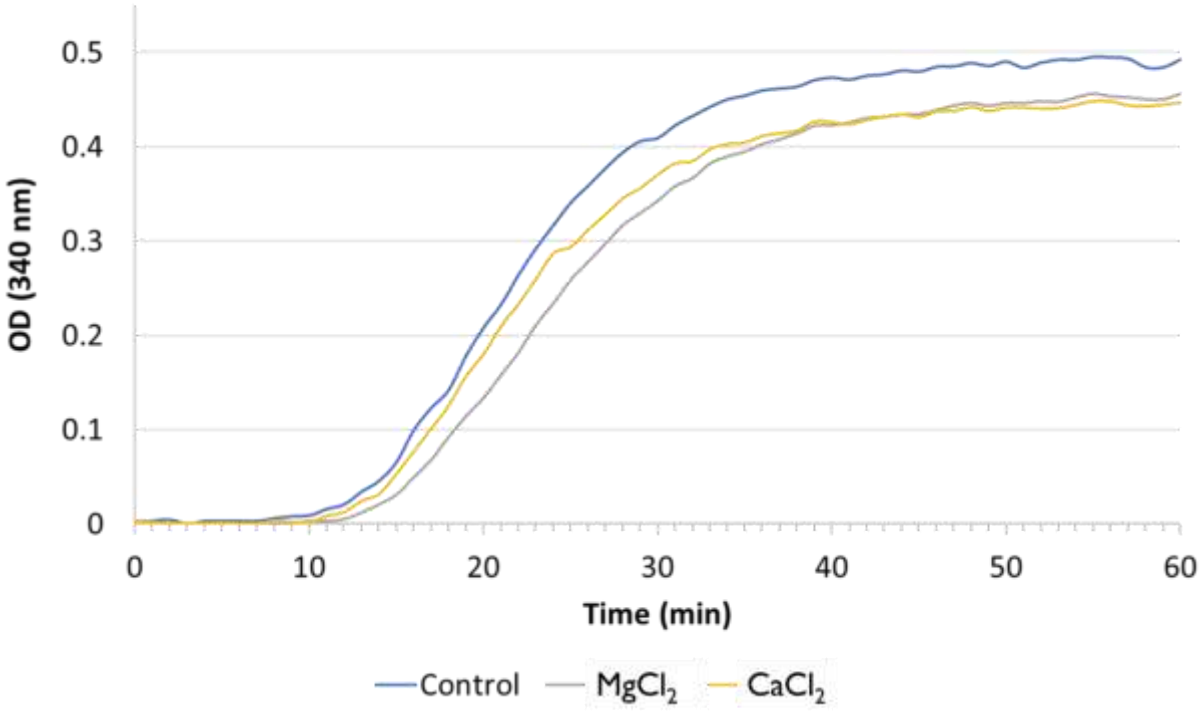

Figure 2.1: Plot of the change in absorbance at 340 nm, as a result of the polymerization of free tubulin into MTs in the presence of GTP and glycerol. As indicated by the legend, three experiments are shown: Control, experiment with added $MgCl_2$ (final concentration Mg^{2+} = 10

μM), experiment with added $CaCl_2$ (final concentration Ca^{2+} = 10 μM). Final concentration of tubulin was 3 mg/mL in a total volume of 110 μL with a temperature jump of 4°C to 37°C. Standard error bars can be seen in Appendix A.

It can be seen in Figure 2.1 that the presence of an additional 10 μM of Mg^{2+} or 10 μM of Ca^{2+} do not increase the polymerization of free tubulin. The results confirm that RPCs are interacting in a way that stabilize microtubules beyond just stabilization due to charge. It suggests that RPCs are interacting with tubulin and/or MTs in a docking or binding manner.

The polymerization of free tubulin *in vitro* in the presence of RPC **2** is shown in Figure 2.2.

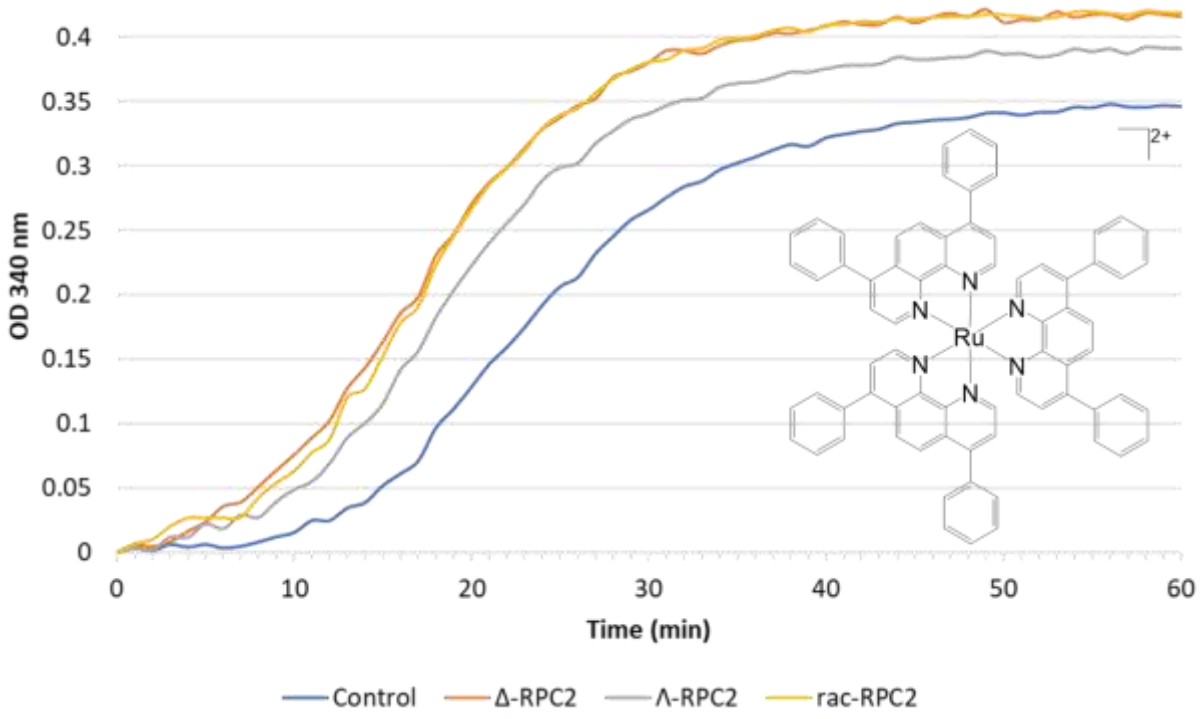

Figure 2.2: Plot of the increasing light-scattering, detected as absorbance at 340 nm, as a result of the polymerization of free tubulin into MTs in the presence of GTP, glycerol, and 10 μM of RPC **2** chloride salt. Final concentration of tubulin was 3 mg/mL in a total volume of 110 μL with a temperature jump of 4°C to 37°C. Standard error bars can be seen in Appendix A.

Figure 2.2 shows that the samples with RPC **2** present seem to have a shorter lag phase, a more rapid polymerization phase, and overall display more overall light scattering than the control. This means that *rac*-RPC **2**, Δ-RPC **2**, and Λ-RPC **2** all polymerize free tubulin into MTs better than the control. Racemic RPC **2** and Δ-RPC **2** seem to polymerize better than Λ-RPC **2**. However, within the errors of this experiment there are no significant differences in MT stabilization by the enantiomers of RPC **2**, meaning, that regardless of which enantiomer of RPC **2** is used, they will polymerize free tubulin similarly.

The polymerization of free tubulin *in vitro* in the presence of RPC **2** is shown in Figure 2.3.

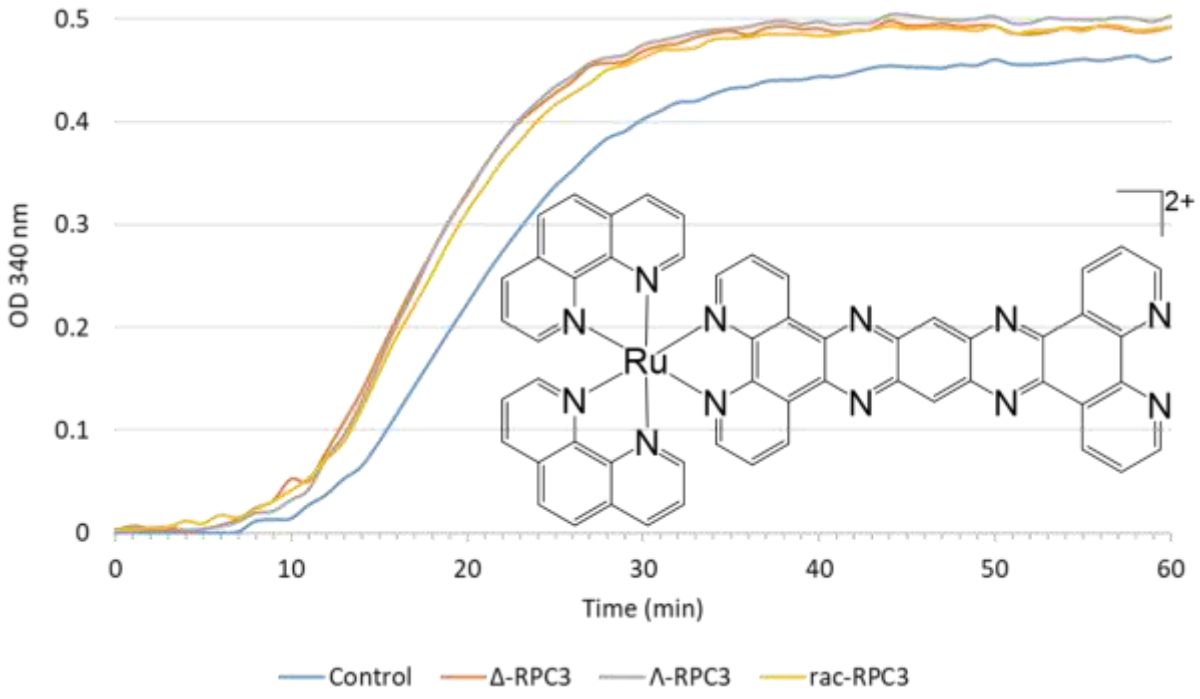

Figure 2.3: Plot of the increasing light-scattering, detected as absorbance at 340 nm, as a result of the polymerization of free tubulin into MTs in the presence of GTP, glycerol, and 10 µM of RPC **3** chloride salt. Final concentration of tubulin was 3 mg/mL in a total volume of 110 µL with a temperature jump of 4°C to 37°C. Error bars can be seen in Appendix A.

In Figure 2.3, the samples with RPC **3** present seem to have a slightly shorter lag phase, a more rapid polymerization phase, and overall display more overall light scattering than the control. This shows that *rac*-, Δ-, and Λ-RPC **3** all polymerize free tubulin into MTs better than the control by almost the same amount. This means that regardless of the chirality of the complex, RPC **3** will polymerize free tubulin similarly.

The plot of the effects of RPC **5** on the polymerization of free tubulin can be seen in Figure 2.4.

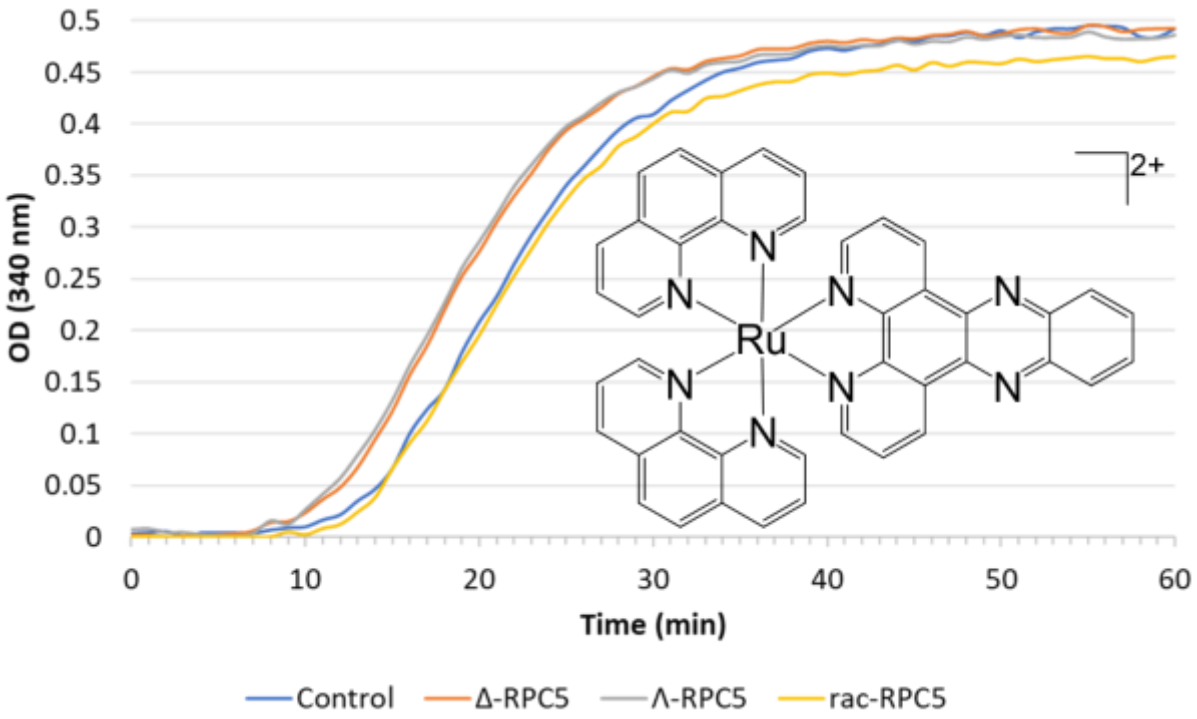

Figure 2.4: Plot of the increasing light-scattering, detected as absorbance at 340 nm, as a result of the polymerization of free tubulin into MTs in the presence of GTP, glycerol, and 10 µM of RPC **5** chloride salt. Final concentration of tubulin was 3 mg/mL in a total volume of 110 µL with a temperature jump of 4°C to 37°C. Error bars can be seen in Appendix A.

Racemic, Δ-, and Λ-RPC **5** do not show a significant difference in polymerization of tubulin compared to the control. It has similar light scattering in the lag phase, polymerization phase, and steady state phase to the control. The racemic RPC **5** seems to be slightly less stabilizing than the enantiopure complexes. However, the chirality of RPC **5** does not play a significant role in MT stabilization within the errors of this experiment. Regardless of what enantiomer of RPC **5** is used, it will have a similar effect on MT stabilization.

As can be seen in Figures 2.2-2.4, the control samples of the plots do not show equal amounts of light scattering. In order to compare RPCs, a summary of the corrected rates and maximum absorbance can be seen in Table 2.1.

Table 2.1 Normalized Summary of MT Polymerization in the Presence of RPCs

Drug	**Polymerization Rate (OD/min)**	**Max OD (340 nm)**	**IC_{50} H358 (μM)**	**Ref.**
Control	0.017	0.350	N/A	
rac-RPC 2	0.023 ± 0.001	0.423 ± 0.019	1.5 ± 0.26	6
Δ-RPC 2	0.022 ± 0.001	0.422 ± 0.087	2.8 ± 0.25	Recent work
Λ-RPC 2	0.021 ± 0.002	0.395 ± 0.013	2.8 ± 0.4	Recent work
rac-RPC 3	0.018 ± 0.001	0.381 ± 0.020	13.2 ± 1.8	6
Δ-RPC 3	0.019 ± 0.0002	0.380 ± 0.009	8.8 ± 1.0	35
Λ-RPC 3	0.020 ± 0.0001	0.390 ± 0.001	13.8 ± 1.5	35
rac-RPC 5	0.015 ± 0.0002	0.322 ± 0.002	35 ± 0.71	6
Δ-RPC 5	0.016 ± 0.001	0.350 ± 0.009	N/A	
Λ-RPC 5	0.017 ± 0.001	0.344 ± 0.003	N/A	

Based on the data collected, there appears to be no significant difference between the enantiomers as all the rates and max absorbances are equal within the error of this experiment. This means that unlike DNA with a physically restricting right-handed major groove, the RPC binding site, whether on the tubulin or polymerized MT, is largely unrestricted. This means that regardless of the enantiomer used, it can stabilize MTs equally.

However, the results are more easily show that the polymerization rates and max absorbances of the RPCs are more strongly correlated to the IC_{50} values of the racemic solutions against H358. RPC **2** is the most cytotoxic and both the racemic and enantiopure versions appear to have a higher polymerization rate and max OD compared to the other two. RPC **3** with the moderate IC_{50}, has a moderate polymerization rate and max OD in turn. RPC **5**, which is the least cytotoxic, also show the least MT stabilization compared to the other two. This suggests that MTs are likely the primary targets of the mononuclear RPCs under study. The difference in cytotoxicity of the enantiomers of RPC **3** suggest that it likely has a different secondary target which is more chiral specific, such as DNA, or it could possibly be related to how the chirality of the complex effects its entry into the cell.[13]

CHAPTER 3. UPTAKE OF RPC 2 INTO H358 CELLS

3.1 Introduction

As discussed in Chapter 2, the IC_{50} value of RPCs against H358 cells is highly correlated to the RPCs' ability to disrupt the MT dynamic. In order to do so, the complex has to first enter the cell and accumulate at the target site. Since RPC **2** has shown to accumulate almost entirely in the cytoskeleton, understanding all aspects of its activity, such as its uptake into the cells, could be key in understanding the time sensitive and dose dependent aspect of this complex as a chemotherapeutic agent. This information would also be very important in enabling us to alter the drug to be more selective against malignant cell lines. The experiment will be an alteration of the one done by Dayoub.[15]

3.2 Experimental Section

3.2.1 Chemicals

The 10x phosphate buffered saline (PBS) was purchased from BioRad and was diluted with Millipore water, adjusted to a pH of 7.4, and autoclaved before use. The sterile and filtered trypsin-EDTA 1x, RPMI-1640 medium, fetal bovine serum (FBS), and penicillin-streptomycin (PS), and trypan blue were purchased from Sigma-Aldrich. The bicinchoninic acid (BCA) was done using the Pierce™ BCA Protein Assay Kit (Cat: 23255) from ThermoFisher. The kit provides 1000 mL of Reagent A which contains sodium carbonate, sodium bicarbonate, bicinchoninic acid and sodium tartrate in 0.1M sodium hydroxide, and 25 mL of Reagent B which contains 4% cupric sulfate. 10x RIPA buffer from Sigma-Aldrich is used for lysis.

3.2.2 Cell Lines and Culture

The H358, human non-small cell lung carcinoma (NSCLC) bronchioalveolar, was obtained from University of Texas Southwestern Medical Center. The H358 was cultured in 60 mm culture plates in RPMI-1640 with 10% FBS and 1% PS at 37°C and 5% CO_2 atmosphere with humidification.

3.2.3 Instrumentation

The cell culture incubator was a ThermoScientific HERACELL 150i CO2 Incubator that was set to 37°C and 5.0% CO_2 with controlled humidity. The centrifuge was an International Clinical Centrifuge Model CL with 115 vac, 50/60Hz and 1.2 amps. The microwave used for cell digestion was the CEM MARS5 Model MARS IP 907005. The settings were as follows: Vessel type: OMNI/XP1500; Control type: Ramp to temperature; Power: 600W - 100%; Ramp: 05:00; PSI: 40; °C control: 130; Hold: 05:00; Av Sample Weight: 0.00 GM; Av Sample Volume: 005 mL. The BGM LABTECH SPECTROstar^{Nano} was used to read the 96-well plate. The wavelength was set to discreate at 562 nm with rapid detection, reading in an antiparallel direction. The Thermofisher-1000 ICP-MS was used to analyze the ruthenium content. The main run was set to sweep jumping of 600 sweeps with a swell time of 10000. The channels were set to detect ^{102}Ru, ^{102}Ru, ^{104}Ru, and ^{115}In with a dwell of 10000 µs and standard resolution. The minimum uptake and wash were set to 0. The maximum uptake was set to 25 and the maximum was set to 120.

3.2.4 Experimental Procedure

A hemocytometer and trypan blue solution is used to count cells prior to seeding. From a full 100 mm culture plate, 2 million H358 cells were counted, and then pipetted into a 60 mm culture plate with 3 mL media. Twelve plates were seeded in this manner and allowed to incubate at 37°C for 24 hours. For the control, 30 µL of the media was removed from three plates and 30 µL of DMSO was in turn added to give a final DMSO concentration of 20 µM. The other plates were treated with 20 µM of *rac*-, Δ-, and Λ-RPC **2** in a similar manner. After 6 hours of treatment at 37°C, the media was removed, and the plates washed 5 times with room temperature PBS. The cells were harvested from the plate by adding 1.5 mL of 37°C 1X trypsin-EDTA and then incubated at 37°C for 10 minutes. The trypsin was neutralized with 1.5 mL media and the suspension pipetted into 15 mL centrifuge tubes. An additional 6 mL of PBS were added to the tubes before they were centrifuged down at setting 3 for 5 minutes. The supernatant was removed, and the pellets washed with 9 mL of PBS three more times. The pellets were then resuspended in 100 µL of 1X RIPA buffer and aliquoted into 2 different microcentrifuge tubes containing 50 µL each. Tube A was used to analyze for the protein content by BCA and Tube B for the ruthenium content by ICP-MS.

Analysis of protein concentration: The resuspended pellets in Tube B were vortexed and sonicated to lyse the cells, and then 40 µL of the suspension was placed into another labelled tube. A solution containing 50:1 ratio of Reagent A to Reagent B from the kit was made, and 360 µL of this solution was added to the cell suspensions to give a total volume of 400 µL; the tubes were then vortexed. Half of the volume was then placed in a covered 96-well plate and then incubated at 37°C for 30 minutes. The plate was then read using a spectrophotometer with a

preexisting calibration curve made using bovine serum albumin (BSA), and the absorbances recorded.

Analysis of ruthenium content: The contents of Tube A were transferred into a XP-1500 plus vessel using 3.5% nitric acid in Millipore water. The volume is brought up to 5 mL with the 3.5% nitric acid. The vessels are then assembled and arranged, and placed in the microwave. The settings should be the same as the one listed above, and one cycle is run. The contents of the vessels were then poured into a new centrifuge tube and the vessel washed into the tube a few times with 3.5% nitric acid. The volume is then brought up to 10 mL, and then sent to the Shimadzu center for ruthenium analysis using the ICP-MS.

3.3 Results and Discussion

Ruthenium was detected in the control samples, so there is a high chance of ruthenium contamination through the microwave process in the XP-1500 vessels. In order to correct this, the ruthenium concentration found in the control was subtracted from all the other samples. The results are plotted in Figure 3.1 which shows the Ru (ng) per million cells.

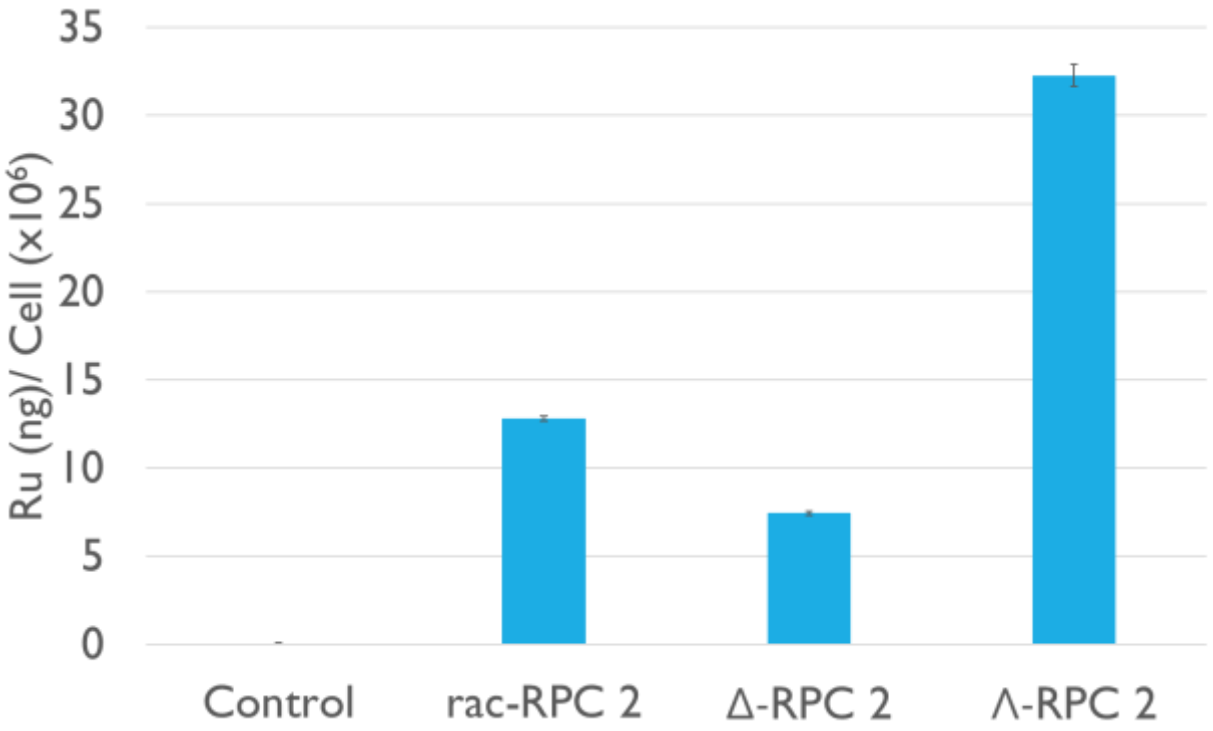

Figure 3.1: Ruthenium content detected using ICP-MS per million cells in H358 cells treated with 20 µM RPC **2** for 6 hours, corrected for ruthenium presence in the control with standard error bars.

From this data, we observe that more than twice as much Λ-RPC **2** enters the cells than the Δ-RPC **2** but a little less than twice as much as the racemic. Their IC_{50} values (*rac*-RPC 2: 1.5 ± 0.26 µM, Δ-RPC 2: 2.8 ± 0.25 µM, Λ-RPC 2: 2.8 ± 0.4 µM) suggest they should have more proportional values, but that is not observed in Figure 3.1 Although all the plates were seeded with the same number of cells, treatment with the drugs cause of lot of cells to die and detach from the plate which can skew the cell count. By lysing the cell and quantifying the protein concentration using the BCA assay, all these errors could be accounted for by normalizing the drug content over the protein concentration eft after the six hour treatment. The plot of ruthenium (ng) per protein content (mg) is shown in Figure 3.2.

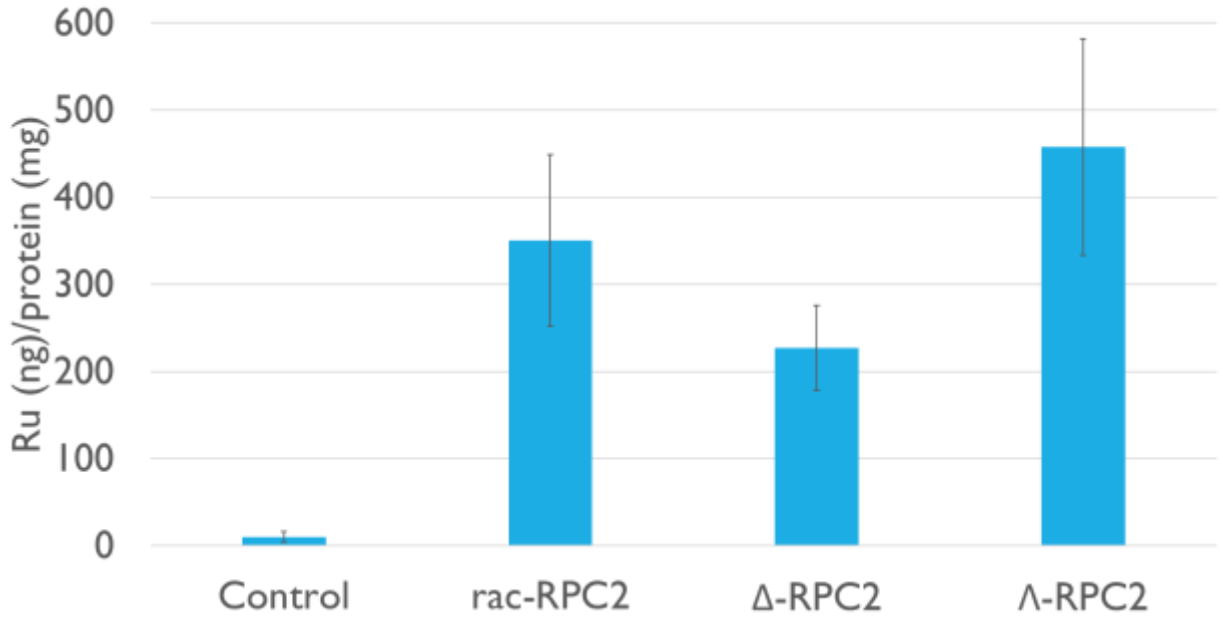

Figure 3.2: Ruthenium content detected using ICP-MS per mg cell protein quantified using BCA in H358 cells treated with 20 µM RPC **2** for 6 hours, corrected for ruthenium presence in the control with standard error bars.

The Λ enantiomer still enters the cell the most, but the standard errors are now within errors of the racemic. The Δ still enters the cell the least, and about half of the Λ, but this time, it is also within error bars of the racemic. The average of the enantiopure samples is almost exactly that of the racemic sample and about twice as much of the Λ enantiomer compared to the Δ enantiomer enters the cell. However, after the 96 hours required to obtain an IC_{50}, enough of the Δ and Λ enantiomers enter the cells to cause the same amount of damage, suggesting the presence of some sort of saturation point. The IC_{50} and 6 hour chiral uptake suggest that the enantiomers in the racemic solution enter the cell independently and the damage caused by the enantiomers are additive.

3.4 Conclusion

While the polymerization assays in Chapter 2 show no significant differences between the enantiomers in MT stabilization, the uptake experiment suggest minor, although not biologically significant differences in the entry of RPC **2** into the cells, as the IC_{50} values of the enantiopure complexes are comparable. However, the ruthenium uptake observed suggests that the enantiomers probably enter the cells at different rates—about 58 $ng \cdot mg^{-1} \cdot h$ for the racemate, 38 $ng \cdot mg^{-1} \cdot h$ for the Δ, and 76 $ng \cdot mg^{-1} \cdot h$ for the Λ—and reached saturation point separately during the duration of the 96 hours to determine the IC_{50}. This could only be explained in that the enantiomers enter the cell through different routes and have alternative cellular targets. If we look at the polymerization data in the previous chapter for RPC **2** and relate it to the IC_{50}, there appears to be a slight advantage for stabilization by the racemate and its IC_{50} is about half of the pure enantiomers. The most likely conjecture is that the Δ and Λ have different binding sites on the tubulin dimer to stabilize MT, since our collaborators have calculated that the racemate has a binding ratio of 1:1 with the number of subunits. It is possible that these sites cause them to stabilize the MTs slightly differently and would explain the similarities between the IC_{50} values of the enantiomers despite the differences in their entry into the cell.

Now, although, RPC **2** showed this uptake trend, RPCs **3** and **4** have greatly differing IC_{50} values which could indicate one of two things, they have different methods of entry that are chiral specific, or they have secondary targets which have chiral preference for interaction. Both are likely to be the case due to the fact that RPCs **3** and **4** show active transport, and the transmembrane transport proteins responsible could easily show chiral preference. They both are also known to cause DSB in cells through ROS generation, and the ROS generated could also

cause mitochondrial membrane depolarization, both of which could show a chiral preference depending on the nature of the docking site. An uptake experiment with the enantiopure complexes of RPCs **3** and **4** would help determine which of these two result in the different IC_{50} values at least in H358 cell lines.

3.5 Recommendation for Future Studies

Other experiments would be to ensure that the drugs are really entering the target site and altering the tubulin the same way in cells by running western blots of cell lines that have been treated with the drugs. The RPCs seem to stabilize MTs in a way other than simple di-cation charge, which suggests the possibility of a binding site. Although our collaborators have observed binding affinities and stoichiometry for RPC **2** to the tubulin dimer, a drug to tubulin binding stoichiometry for the other RPCs are still needed to strengthen the proposition that there is a clear binding site. A binding site study could also be used to confirm that the RPC **2** enantiomers indeed have different binding sites, and which enantiomer is inhibited by paclitaxel. If this is proven to be true, it would explain why RPC **2** has been observed to stabilize MT better than paclitaxel. Another way to be entirely certain of a binding site is to get the x-ray crystallography of the drug binding to either free tubulin or polymerized MTs. Finally, since confocal microscopy have shown that many cells get stuck at late anaphase to early telophase due to the disruption of the MT dynamic, a statistical spread of where the cell cycle is attenuated using flow cytometry could determine whether this occurrence is statistically significant.

CHAPTER 4. RESOLUTION OPTIMIZATION OF [RU(PHEN)$_2$PHENDIONE]CL$_2$ AND RPC 2

4.1 Introduction

Most biological molecules exhibit chirality, such as preference for D-sugars, L-amino acids, right-handed B-DNA, which could all play a role in how chiral drugs interact with their resulting structures. In which case, it becomes important to be able to test these chiral interactions by resolving the enantiomers and running tests with enantiopure drugs. Since resolving the [Ru(phen)$_2$phendione]$^{2+}$ starting material of RPCs **3**-**5** allows for highly pure asymmetrical synthesis of these complexes, optimization of this resolution is highly sought after. Although, arguably, Ru(phen)$_2$Cl$_2$ is an even earlier starting material that could allow for an even greater variety of asymmetric synthesis, the fact that it has the dichlorides makes it less stable than the tris polypyridine substituted [Ru(phen)$_2$phendione]$^{2+}$. RPC **2** is a different product all on its own and has to be resolved as is. However, the lipophilicity of it, makes it hard to resolve in the same manner as the [Ru(phen)$_2$phendione]$^{2+}$.

One way to optimize resolution is to optimize the synthesis of the resolving salts. The syntheses for the resolving salts in literature exist for sodium arsenyl tartrate and potassium antimonyl tartrate.[30] However, yields for potassium antimonyl tartrate are generally low due to solubility issues and large batches cannot be easily made. Potassium antimonyl tartrate also requires a high energy of solvation which can make resolution difficult. The MacDonnell lab has previously tried synthesizing sodium antimonyl tartrate which dissolves more readily in water. However, the resulting salt had low purity because it does not readily recrystallize like the other two metal tartrates.

Another way to optimize the resolution is to use less reagents. Previously, the metal tartrate salts were used in excess. A 1:1 stoichiometric ratio has not been tried to resolve $[Ru(phen)_2phendione]Cl_2$ and RPC **2**. In this chapter, two things are conjectured: (A) the use of a 1:1 ratio of RPC to resolving salt is sufficient for resolution; and (B) the use of a smaller more hydrated sodium arsenyl (II) tartrate will better resolve hydrophilic complexes, such as $[Ru(phen)_2phendione]^{2+}$, under more hydrophilic environments, while the larger less hydrated sodium antimonyl (II) tartrate will better resolve lipophilic complexes, such as RPC **2**, under more lipophilic environments. The resolution route will be a derivation of the one done by Sun *et al.* as seen in Scheme 4.1.[28]

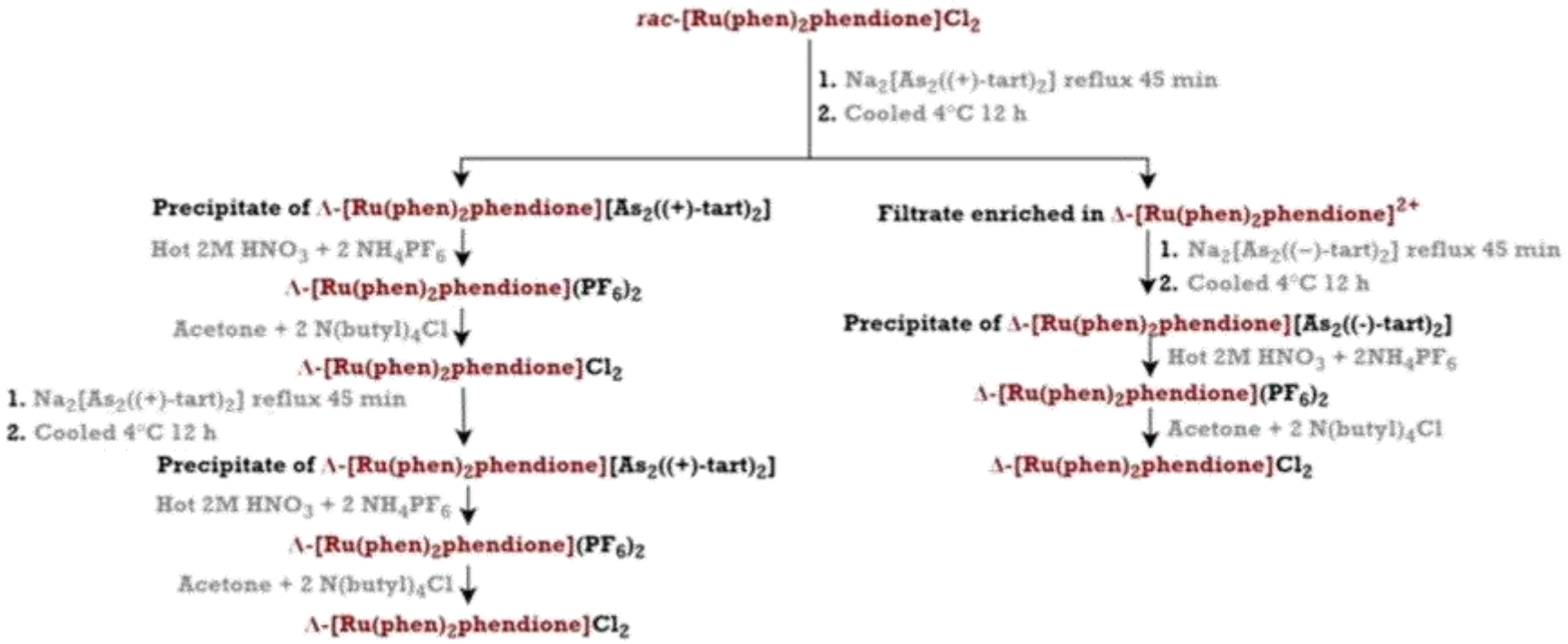

Scheme 4.1: Resolution route of [Ru(phen)$_2$phendione]Cl$_2$

4.2 Experimental Section

4.2.1 Chemicals

All reagents and solvents were reagent grade and used as is unless specified. Many reagents and solvents from varying vendors were used. Enantiopure sodium arsenyl tartrate salts, $Na_2[As_2tart_2]$, were made as directed by Scalessinger et al. Sodium antimonyl tartrate, $Na_2[Sb_2tart_2]$, and potassium antimonyl tartrate salts, $K_2[Sb_2tart_2]$, were made in a similar manner.[30] 1,10-Phenanthroline-5,6-dione (phendione) was synthesized as per literature.[31] $Ru(phen)_2Cl_2$, and $[Ru(phen)_2phendione](PF_6)_2$, and $[Ru(DIP)_3](PF_6)_2$ were synthesized with a method derived from the literature.[32-34] HPLC grade methanol and acetonitrile were used for the analytical chiral high performance liquid chromatography (HPLC).

4.2.2 Instrumentation

The polarimeter used to determine optical rotation was Jasco P-1010. The cell length is 100.00 mm with a concentration of 0.1000 (w/v%). Jeol Eclipse Plus 500 MHz Spectrometer was used to obtain proton NMRs using D_2O solvent and 2,2-Dimethyl-2-silapentane-5-sulfonic acid (DDS) as the zero ppm standard. The melting points of the metal tartrate salts were taken using differential scanning calorimetry (DSC) with the Shimadzu DSC-60 using the TA-60WS program. The pan used was aluminum under nitrogen flowed into the cell at a rate of 20 mL/min.

4.2.3 Optimization of the Synthesis of Sodium Antimonyl Tartrate, $Na_2[Sb_2C_8H_8O_{12}]$

In an Erlenmeyer flask, 15 g (0.1 mol) of L(+)-tartaric acid was dissolved in 25 mL DI water. Antimony (III) oxide, 14.58 g (0.05 mol), was added to this solution and heated gently while

stirring. In another flask, 4 g (0.1 mol) of sodium hydroxide was dissolved in 25 mL water and the solution brought to a boil. The sodium hydroxide solution was added dropwise to tartaric acid and antimony (III) oxide solution over 10 minutes. The reaction was then digested at 300°C until only ~0.05 g of antimony (III) oxide was left. The reaction was filtered hot and the filtrate was allowed to slowly cool to room temperature. The solution was then stored overnight at 4°C. The next day, 30 mL ethanol was added to the solution resulting in a cloudy solution. The precipitate was vacuum filtered and washed first with 100 mL of cold 50:50 DI water:ethanol and then with ethanol until the wash was clear. The crystals were then recrystallized in 50:50 water:ethanol. Precipitate was allowed to dry in 50°C vacuum oven overnight to remove the hydrates. The D(-) salt was made the same way with D-tartaric acid, yielding L(+) = 91% (26.69 g) and D(-) = 91% (26.77 g). ^{1}H NMR (D_2O) δ = 4.52 (s, 2H, CH). $[\alpha]_D^{20}$(c = 0.10, H_2O) L(+) = +150°. $[\alpha]_D^{20}$(c = 0.10, H_2O) D(-) = -147°. MP L(+): 165-170°C. MP D(-): 146-148°C.

4.2.4 Optimization of the Synthesis of Potassium Antimonyl Tartrate, $K_2[Sb_2C_8H_8O_{12}]$

In an Erlenmeyer flask, 15 g (0.1 mol) of L(+)-tartaric acid was dissolved in 25 mL DI water. Antimony (III) oxide, 14.58 g (0.05 mol), was added to this solution and heated gently with stirring. In another flask, 5.61 g (0.1 mol) of potassium hydroxide was dissolved in 25 mL water and the solution brought to a boil. The sodium hydroxide solution was added dropwise to tartaric acid and antimony (III) oxide solution over 10 minutes. The reaction was then digested at 300°C until only ~0.2 g of antimony (III) oxide was left. The reaction was filtered hot and the filtrate was allowed to slowly cool to room temperature. The solution was then stored overnight at 4°C. The precipitate was vacuum filtered and washed with cold DI water until wash was clear. The crystals

were then recrystallized in DI water. Precipitate was allowed to dry in 50°C vacuum oven to dehydrate. The D(-) salt was made the same way with D-tartaric acid, yielding L(+) = 89% (27.48 g) and D(-) = 85% (26.20 g). ^{1}H NMR (D_2O) δ = 4.52 (s, 2H, CH). $[\alpha]_D^{20}$(c = 0.10, Millipore H_2O) L(+) = +138°. $[\alpha]_D^{20}$(c = 0.10, Millipore H_2O) D(-) = -144°. MP L(+): 246-252°C. MP D(-): 238-250°C.

4.2.5 Optimization of the Resolution of $[Ru(phen)_2phendione]Cl_2$

Four samples of 0.5 g ($6.7x10^{-4}$ mol) of $[Ru(phen)_2phendione]Cl_2$ were dissolved in 25 mL DI water with stirring. One stoichiometric equivalent of either $Na_2[As(+)tart_2]$, $Na_2[As(-)tart_2]$, $Na_2[Sb(+)tart_2]$, or $Na_2[Sb(-)tart_2]$ were dissolved in 10 mL water. Both solutions were brought up to 80°C and then mixed together. The solution was allowed to stir vigorously 80°C for 45 minutes. Once precipitates were visible, the flask was covered in parafilm and refrigerated (4°C) overnight. The $[Ru(phen)_2phendione]$ metal tartrate precipitate was then filtered under vacuum. The precipitate was then dissolved in 30 mL of hot 2 M nitric acid and stirred vigorously at 100°C for one hour. The solution was allowed to cool and the $[Ru(phen)_2phendione]^{2+}$ was precipitated with excess NH_4PF_6. The resulting precipitate was then filtered under suction and about 2 mg was sent to the Shimadzu lab to check for enantiopurity using chiral HPLC and the resolved enantiomer was checked via circular dichroism (CD) in acetonitrile.

4.2.6 Optimization of the Resolution of RPC 2, $[Ru(DIP)_3]Cl_2$

Four samples of 0.5 g ($4.3 x10^{-4}$ mol) of $[Ru(DIP)_3]Cl_2$ were dissolved in 25 mL ethanol with stirring. One stoichiometric equivalent of either $Na_2[As(+)tart_2]$, $Na_2[As(-)tart_2]$, $Na_2[Sb(+)tart_2]$, or $Na_2[Sb(-)tart_2]$ were dissolved in 10 mL water. Both solutions were brought up to 80°C and

then mixed together. The solutions were allowed to stir vigorously at 80°C until everything dissolved. Drops of DI water were added to the flask until precipitates formed. The solution was allowed to stir vigorously as it cooled. The flask was then covered in parafilm and placed in the freezer (-20°C) for one hour. The $[Ru(DIP)_3]$ metal tartrate precipitate was then filtered under vacuum. The precipitate was then dissolved in 30 mL of hot 2 M nitric acid and stirred vigorously at 100°C for 10 minutes before adding 30 mL of ethanol. After 30 minutes of vigorous stirring at 100°C, the $[Ru(DIP)_3]^{2+}$ was then precipitated with excess NH_4PF_6 and allowed to continue stirring for another 30 minutes. The suspension was then allowed to cool. The resulting precipitate was then filtered under suction and about 2 mg was sent to the Shimadzu lab to check for enantiopurity using chiral HPLC and the resolved enantiomer was checked via CD in acetonitrile.

4.3 Results and Discussion

The syntheses of the metal tartrate salts were successfully optimized with yields increasing to 90% for sodium antimonyl tartrate and 85% for potassium antimonyl tartrate, the optical purity increasing to >90%. The optimized methods for synthesis of the metal tartrates prevent the accidental racemization of the tartaric acid that occurred at higher temperatures using the method described by Sun et al. The reported specific rotation for $Na_2[As_2(+)tart_2]$ is +85.5°, while the experimental rotation value was +77°.[30] Assuming the conditions that the optical rotation was taken in was the same, the $[As_2(+)tart_2]^{2-}$ salt was 90% optically pure while the D(-) salt was only 84% optically pure. However, the salts are comparable as the optical rotation of the $[Sb_2tart_2]^{2-}$ salts are consistently twice the value of the $[As_2tart_2]^{2-}$ counterpart.

Table 4.1 provides a summary of the resolution. The percent enantiomeric excess (%ee) was calculated using the peak area from the chiral HPLC elution profile.

Table 4.1. Resolution Summary

Salt	$Na_2[As_2tart_2]$ 1:1		$Na_2[Sb_2tart_2]$ 1:1		$Na_2[As_2tart_2]$ 1:1		$Na_2[Sb_2tart_2]$ 1:1	
	L	D	L	D	L	D	L	D
	$[Ru(phen)_2phendione]Cl_2$				$[Ru(DIP)_3]Cl_2$			
Λ %Yield	68%		64%			91%		71%
Λ %ee	96%		0%			61%		94%
Δ %Yield		68%		56%	51%		67%	
Δ %ee		78%		0%	0%		67%	

As shown in Scheme 4.1, previously, the precipitate had to be resolved twice to obtain over 90%ee. However, Table 4.1 shows that under the conditions discussed in this chapter, it is possible to obtain >90%ee of the Λ enantiomers after only the first resolution of the precipitate with appreciable yields of >200 mg. The conditions discussed also allow for the Δ enantiomer to be resolved first, which was not practical previously. The data collected supports that a 1:1 ratio can successfully resolve the RPC. In fact, it shows that having excess resolving salt can actually be detrimental to the enantiopurity of the RPC. This is very good news since that means we can use less resolving salt in the future.

The data collected also supports the hypothesis that the more hydrophilic $[Ru(phen)_2phendione]^{2+}$ would be better resolved by the more hydrophilic $[As_2tart_2]^{2-}$ under

hydrophilic environments. One could argue that the L salt was better at resolving the $[Ru(phen)_2phendione]^{2+}$ than the D salt the L-tartaric acid is the naturally occurring acid and to some extent probably more stable than the D-tartaric acid. However, this is not true when it comes to resolving RPC **2**. The metal L-tartrate salt did not resolve as well as the D-tartrate salt. In fact, the results of the resolution of RPC **2** were entirely unexpected. The L-tartrate precipitated the Δ RPC and the D-tartrate precipitated the Λ RPC, the reverse of what is expected based on the resolution of the fully characterized RPC **1**. The Λ-RPCs appear to precipitate easier from aqueous solvent systems and this could possibly be used to our advantage in the future by obtaining the Δ RPC by removing all the Λ RPC from the solution.

Another observation that was made, was that the solvent system itself is crucial to the separation. Previous resolution attempt of RPC **2** by the MacDonnell lab resulted in the D-tartrate precipitated the Δ RPC and the L-tartrate precipitated the Λ RPC. However, the resolving conditions were 50:50 ethanol:water using excess resolving salt. When using this solvent system with the synthesized resolving salts, it resulted in all the diastereomers precipitating out of solution. When using 100% ethanol, it resulted in all the diastereomers remaining in solution, which is how the conditions discussed in the experimental section came to fruition. This suggests that the solvent system can determine which enantiomer of the RPC stays in solution. This could be a groundbreaking discovery if the solvent system can truly determine the precipitation order because it means that everything can be precipitated by the L-tartrate salt. The D-tartrate salt is more expensive to make, therefore, using only the L salt would save a lot of money.

REFERENCES

1. Balzani, V.; Juris, A. *Coordin. Chem. Rev.*, **2001**, *211*(1), 97-115.
2. Tan, T.N.; Weston, R.H.; Hogan, J.P. *Appl. Radiat. Isot.*, **1971**, *22*(5), 301-308.
3. Komor, A. C.; Barton, J.K. *Chem. Commun.*, **2013**, *49*(35), 3617-3630.
4. Barton, J.K. *J. Am. Chem. Soc.*, **1984**, *106*, 2172-2176.
5. Dwyer F.P.; Gyarfas, E.C.; Rogers, W.P.; Koch, J.H. *Nature*, **1952**, *170*(4318), 190-191.
6. Alatrash, N.; Narh, E. S.; Yadav, A.; Kim, M. J.; Janaratne, T.; Gabriel, J.; MacDonnell, F. M. *Chem. Med. Chem.*, **2017**, *12*, 1055-1069.
7. Dvir, H.; Silman, I.; Harel, M.; Rosenberry, T. L.; Sussman, J. L. *Chem. Biol. Interact.*, **2010**, *187*(1-3), 10-12.
8. Hambley, T.W. *J. Chem. Soc., Dalton Trans.,* **2001**, *19,* 2711-2718.
9. Muhammad, N.; Guo, Z. *Curr. Opin. Chem. Biol.*, **2014**, *19*, 144-153.
10. Chen, J.; Chen, L.; Liao, S.; Zheng, K.; Ji, L. *J. Phys. Chem.*, **2007**, *111*, 7862-7869.
11. Bijelic, A.; Theiner, S.; Kepplet, B.K.; Rompel, A. *J. Med. Chem.*, **2016**, *56*, 5894-5903.
12. Barry, N.P.E.; Sadler, P.J. *Chem. Soc. Rev.*, **2012**, *41*, 3264–3279.
13. Griffith, C.; Dayoub, A. S.; Jaranatne, T.; Alatrash, N.; Mohamedi, A.; Abayan, K.; Breitbach, Z. S.; Armstrong, D. W.; MacDonnell, F. M. *Chem. Sci*, **2017**, *8*, 3726-3740.
14. Friedman, A. E.; Chambron, J. C.; Sauvage, J. P.; Turro, N. J.; Barton, J. K. *J. Am. Chem. Soc.*, **1990**, *112*, 4960-4962.
15. Dayoub, A.S.; Mohamedi, A.; Dominguez, A.T.A.; Toombs, J.E.; Shelor, C.P.; Alatrash, N.; Burton, N.; Brekken, R.A.; MacDonnell, F.M. *Chem Biochem*., **2019** (Under Review).

16. Dickerson, M.; Sun, Y.; Howerton, B.; Glazer, E. C. *Inorg. Chem.*, **2014**, *53*, 10370-10377.

17. Goldstein, B. M.; Barton, J. K.; Berman, H. M. *Inorg. Chem.*, **1986**, *25*, 842-847.

18. Ortega, A. L.; Mena, S.; Estrela, J. M. *Cancers*, **2011**, *3*(1), 1285-1310.

19. Jakubaszek, M.; Goud, B.; Ferrari, S.; Gasser, G. *Chem. Comm.*, **2018**, *54*, 13040-13059.

20. Pierroz, V.; Joshi, T.; Leonidova, A.; Mari, C.; Schur, J.; Ott, I.; Spiccia, L.; Ferrari, S.; Casser, G. *J. Am. Chem. Soc.*, **2012**, *134*, 20376-20387.

21. Fong, J.; Kasimova, K.; Arenas, Y.; Kaspler, P.; Lazic, A.; Mandel, A.; Lilge, L. *Photochem. Photobiol. Sci.*, **2015**, *14*, 2014-2023.

22. Long, B. H.; Fairchild, C. R. *Cancer Res.*, **1994**, *54*, 4355-4361.

23. Barenjee, S.; Hwang, D. J.; Li, W.; Miller, D. D. *Molecules*, **2016**, *21*, 1468.

24. Blajeski, A. L.; Phan, V. A.; Kottke, T. J.; Kaufmann, S. H. *J. Clin. Invest.*, **2002**, *110*, 91-99.

25. Mooberry, S. L.; Tien, G.; Hernandez, A. H.; Plubrukarn, A.; Davidson, B. S. *Cancer Res.*, **1999**, *59*, 653-660.

26. Larsson, H.; Wallin, M.; Edström, A. *Exp. Cell Res.*, **1976**, *100*, 104-110.

27. Olmsted, J. B.; Borisy, G. G. *Biochem.*, **1975**, *14*(13), 2996-3005.

28. Sun, P.; Krishnan, A.; Yadav, A.; Singh, S.; MacDonnell, F.M.; Armstrong, D.W. *Inorg. Chem.,* **2007**, *46*, 10312-10320.

29. Kim, M. J.; Konduri, R.; Ye, H.; MacDonnell, F. M.; Puntoriero, F.; Serroni, S.; Campagna, S.; Holder, T.; Kinsel, G.; Rajeshwar, K. *Inorg. Chem.*, **2002**, *41*, 2471-2476.

30. Scalessinger, G.; Parry, R. W. In *Inorganic Syntheses*; Gebala, A. E., Jones, M. M., Eds.; McGraw-Hill Book Company, Inc., 1970; Vol. XII, pp 267–269.

31. Inglett, G. E.; Smith, F. *J. Am. Chem. Soc.*, **1950**, *72*, 842-844.

32. Sullivan, B. P.; Salmon, D. J.; Meyer, T. J. *Inorg. Chem.*, **1978**, *17*(12), 3334-3341.

33. Alatrash, A.; Narh, E. S.; Yadav, A.; Kim, M. J.; Janaratne, T.; Gabriel, J.; MacDonnell, F. M. *Chem. Med. Chem.*, **2017**, *12*, 1-16.

34. Watts, R. J.; Crosby, G. A. *J. Am. Chem. Soc.*, **1971**, *93*(13), 3184-3188.

35. Yadav, A.; Janaratne, T.; Krishnan, A.; Sighal, S. S.; Yadav, S.; Dayoub, A. S.; Hawkins, D. L.; Awasthi, S.; MacDonnell, F. M. *Mol. Cancer Ther.*, **2013**, *12*(5), 1-20.

APPENDIX A

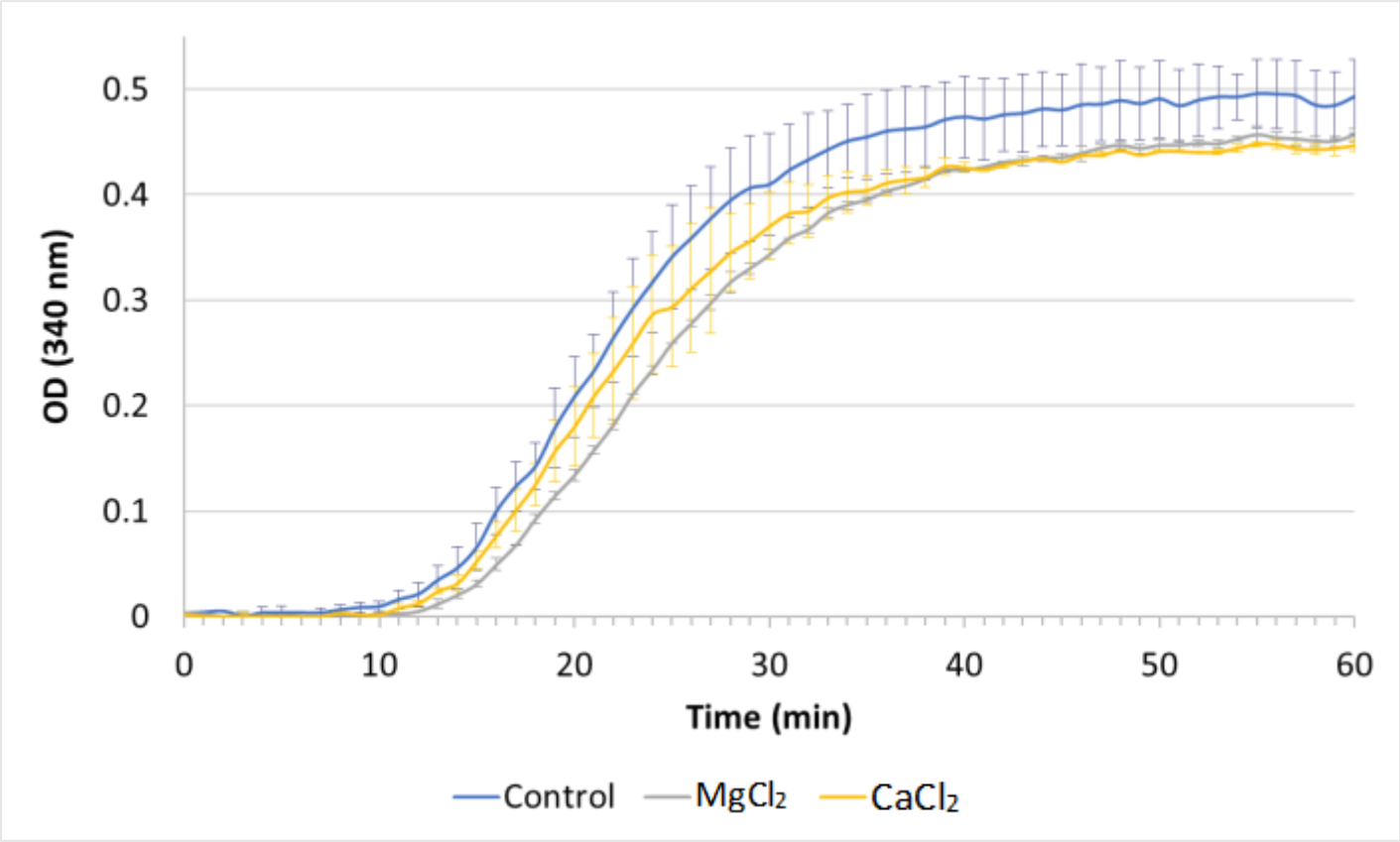

Plot with standard errors of the change in absorbance at 340 nm, as a result of the polymerization of free tubulin into MTs in the presence of GTP and glycerol. As indicated by the legend, three experiments are shown: Control, with $MgCl_2$ added (final concentration Mg^{2+} = 10 µM), with $CaCl_2$ added (final concentration Ca^{2+} = 10 µM). Final concentration of tubulin was 3 mg/mL in a total volume of 110 µL with a temperature jump of 4°C to 37°C.

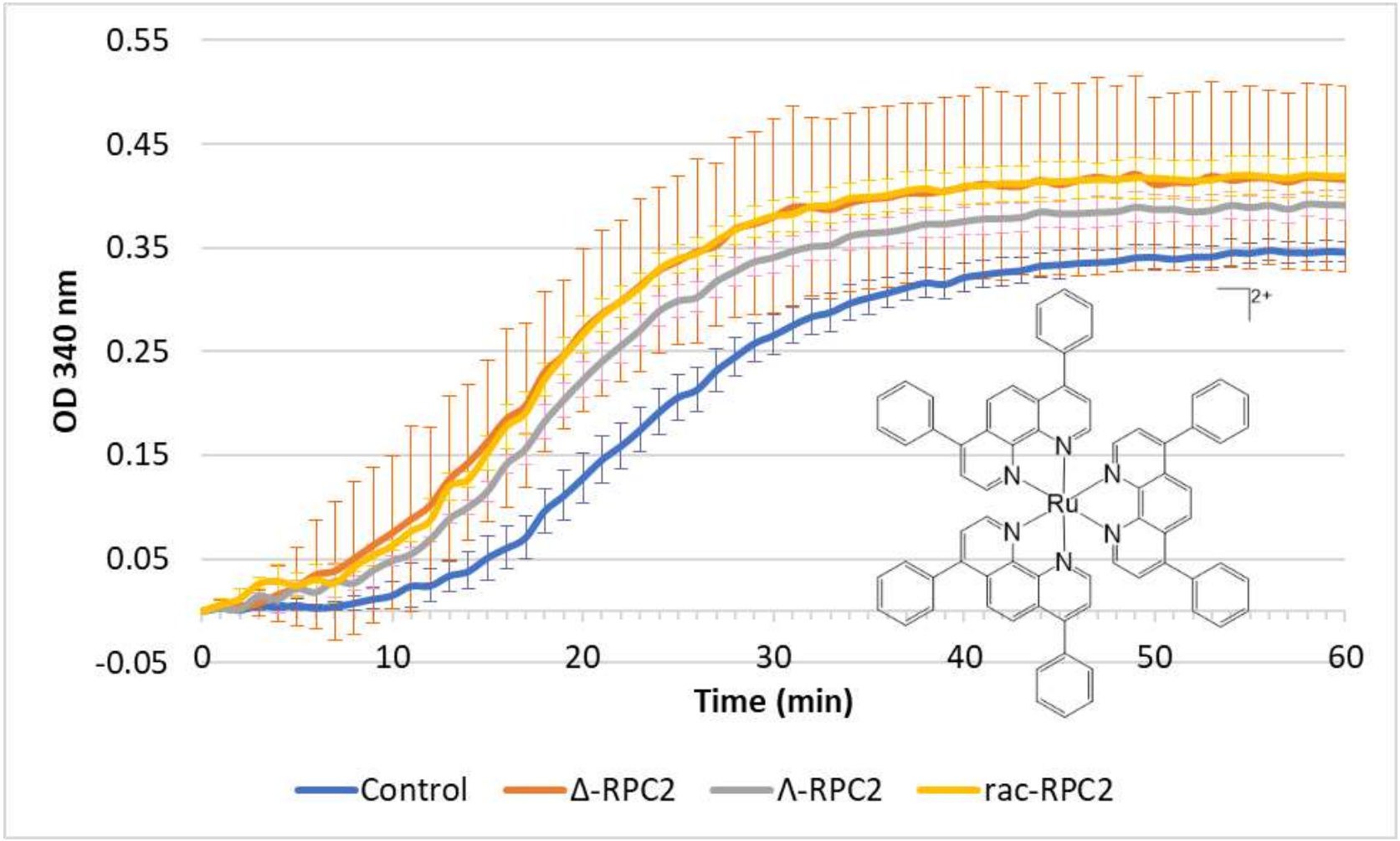

Plot with the standard errors of the increasing light-scattering, detected as absorbance at 340 nm, as a result of the polymerization of free tubulin into MTs in the presence of GTP, glycerol, and 10 µM of RPC **2** chloride salt. Final concentration of tubulin was 3 mg/mL in a total volume of 110 µL with a temperature jump of 4°C to 37°C.

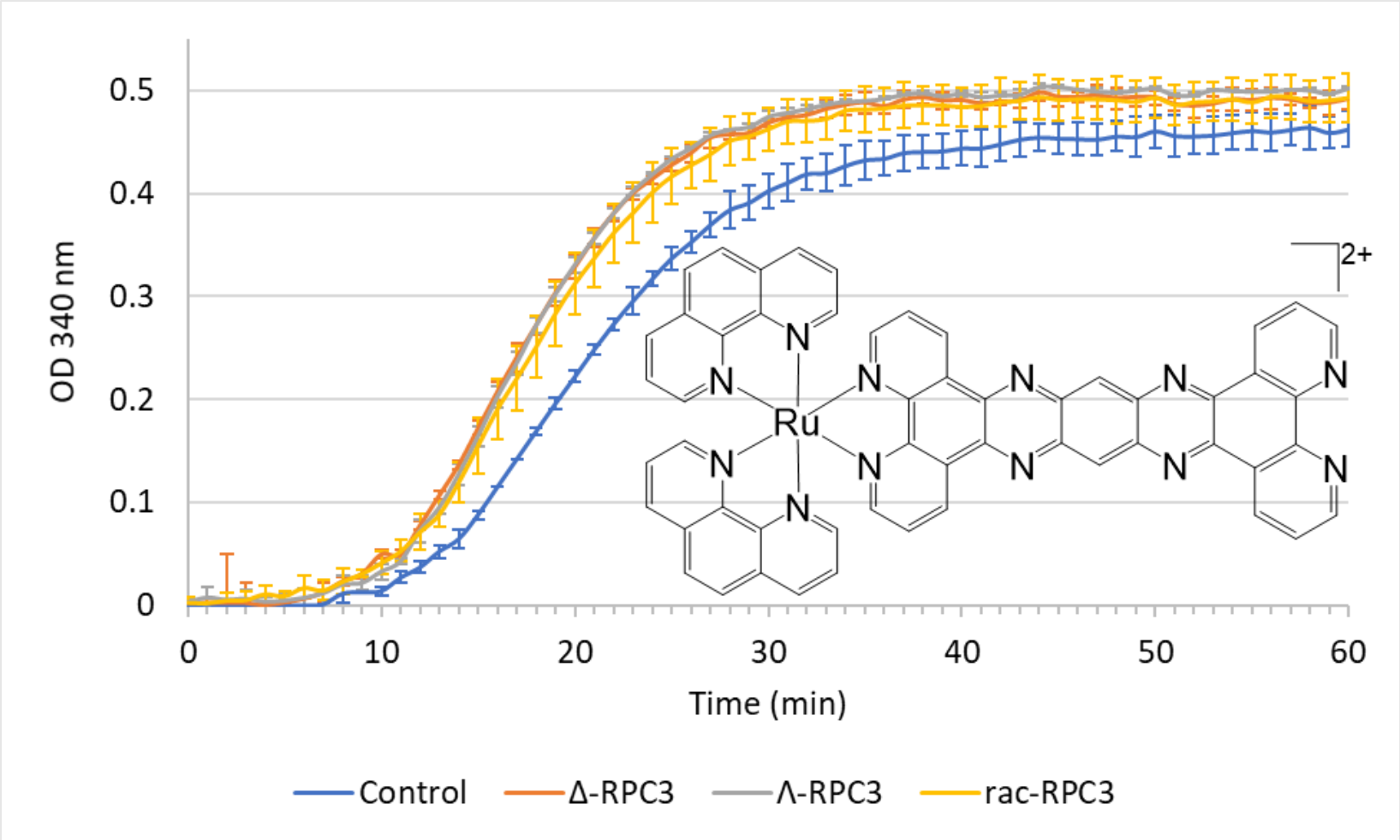

Plot with the standard errors of the increasing light-scattering, detected as absorbance at 340 nm, as a result of the polymerization of free tubulin into MTs in the presence of GTP, glycerol, and 10 µM of RPC **3** chloride salt. Final concentration of tubulin was 3 mg/mL in a total volume of 110 µL with a temperature jump of 4°C to 37°C.

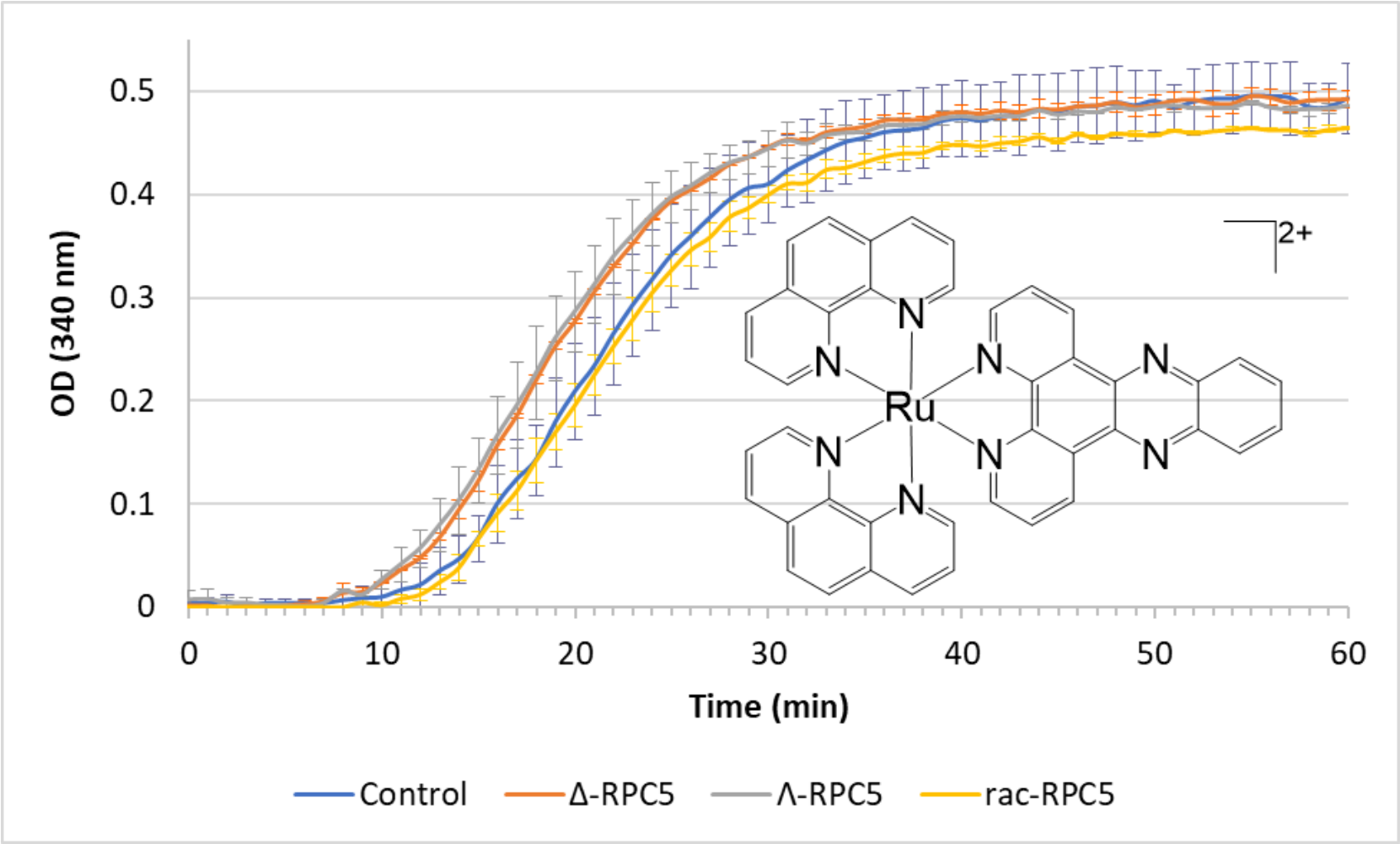

Plot with the standard errors of the increasing light-scattering, detected as absorbance at 340 nm, as a result of the polymerization of free tubulin into MTs in the presence of GTP, glycerol, and 10 µM of RPC **5** chloride salt. Final concentration of tubulin was 3 mg/mL in a total volume of 110 µL with a temperature jump of 4°C to 37°C.

APPENDIX B

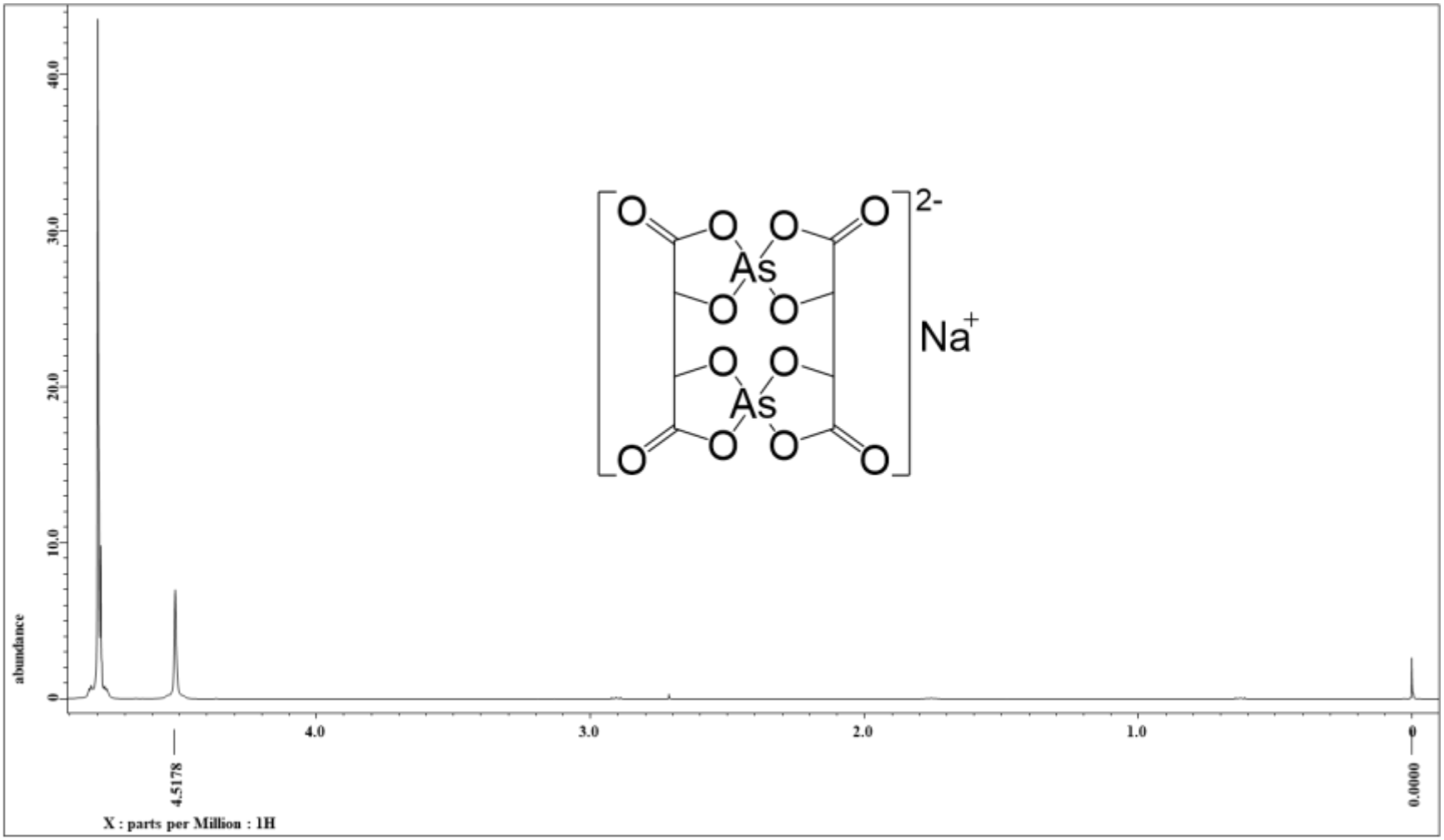

^{1}H NMR Spectrum of $Na_2[As_2C_8H_8O_{12}]$ in D_2O

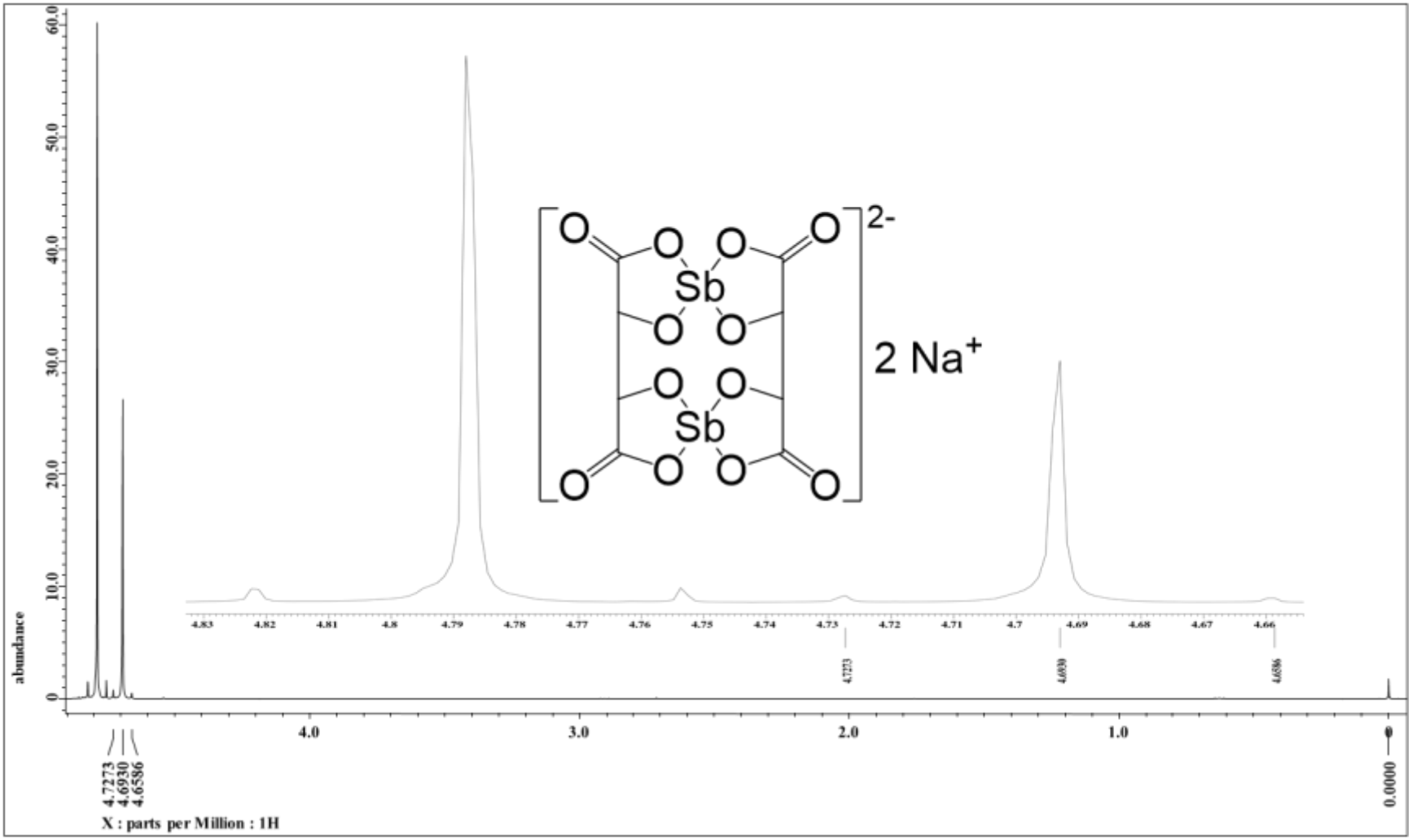

^{1}H NMR Spectrum of $Na_2[Sb_2C_8H_8O_{12}]$ in D_2O

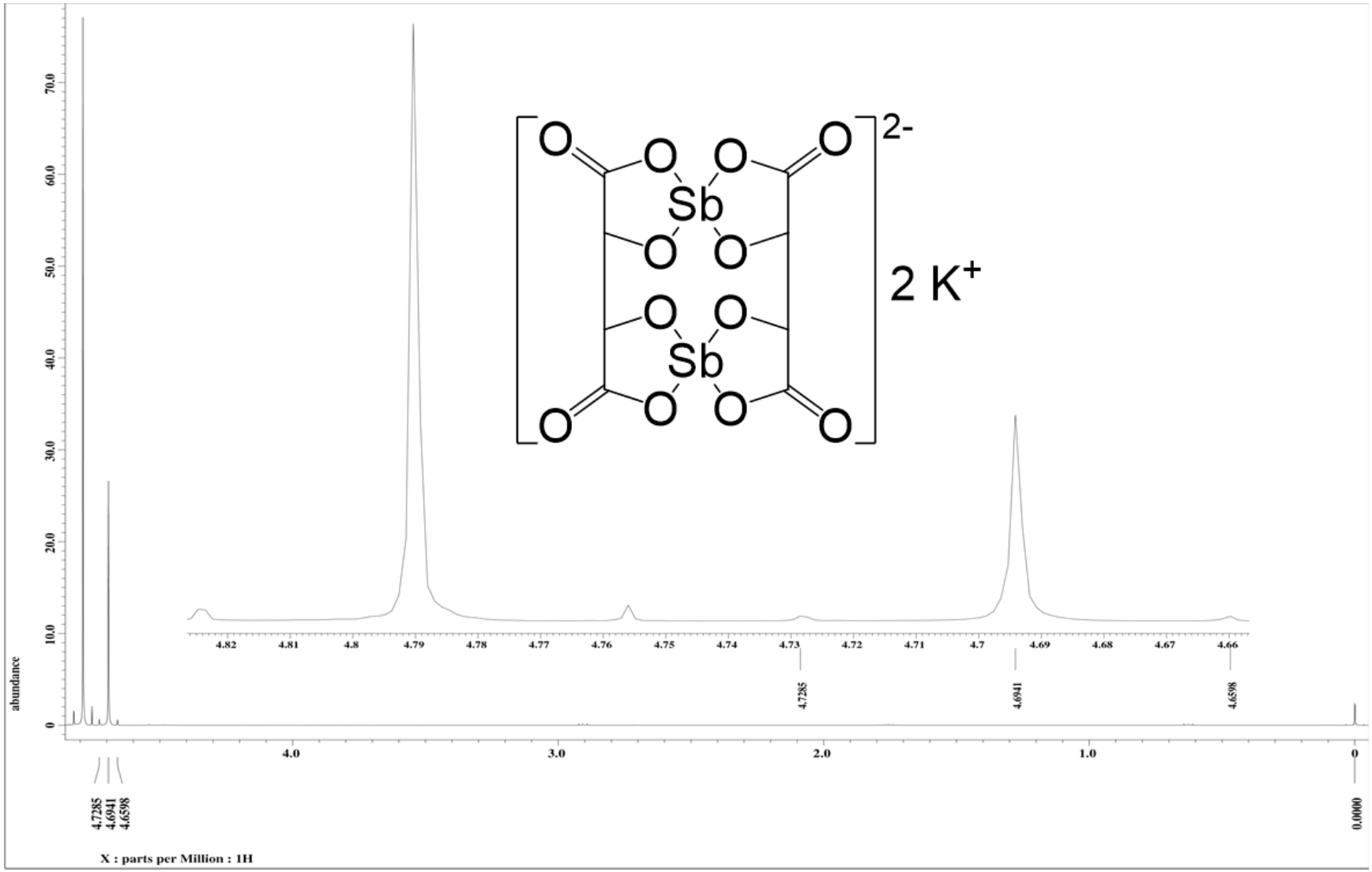

^{1}H NMR Spectrum of $K_2[Sb_2C_8H_8O_{12}]$ in D_2O

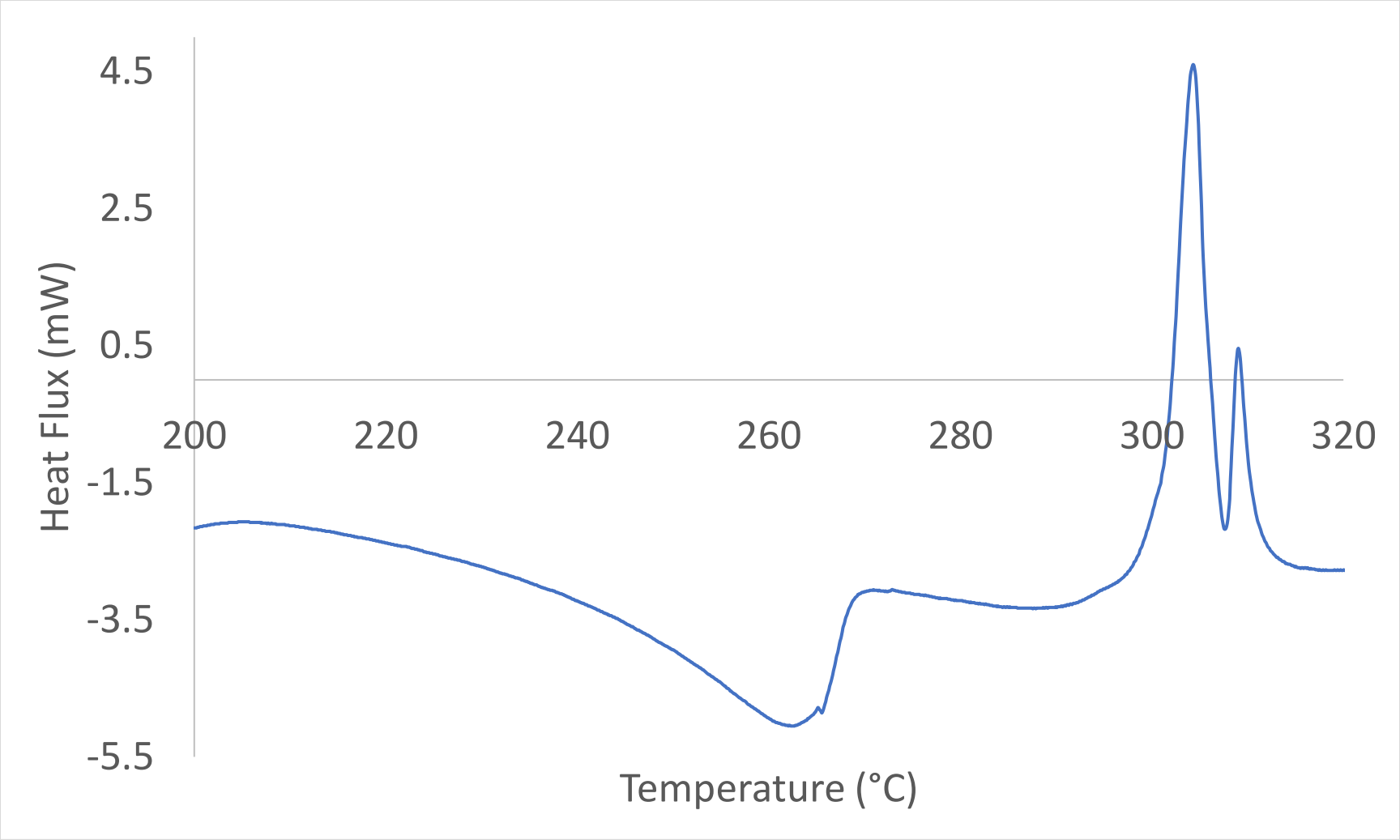

Melting profile of $Na_2[As_2\text{-}L(+)\text{-}C_8H_8O_{12}]$ at a ramp rate of 5°C per minute under N_2 atmosphere in aluminum pans.

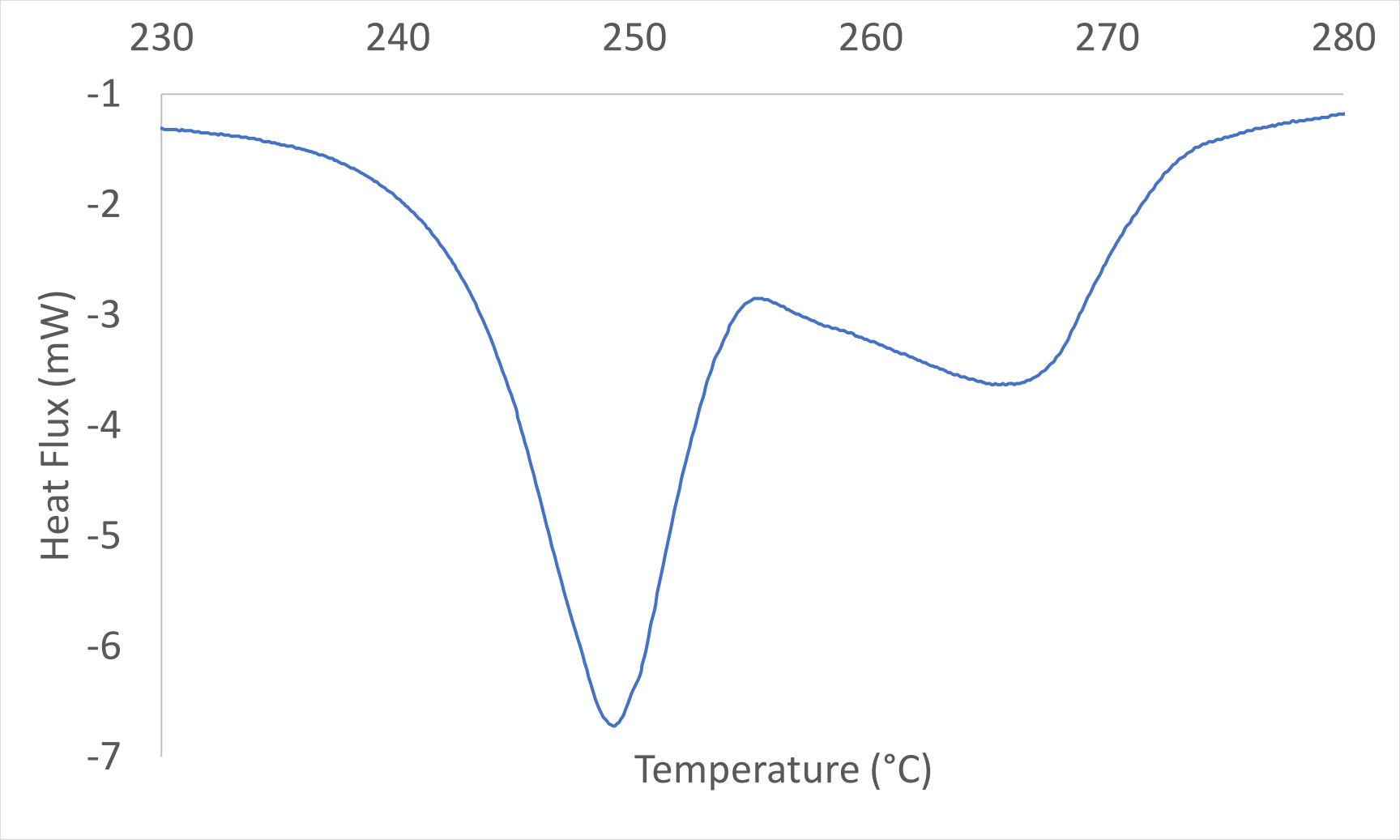

Melting profile of $Na_2[As_2\text{-}D(-)\text{-}C_8H_8O_{12}]$ at a ramp rate of 5°C per minute under N_2 atmosphere in aluminum pans.

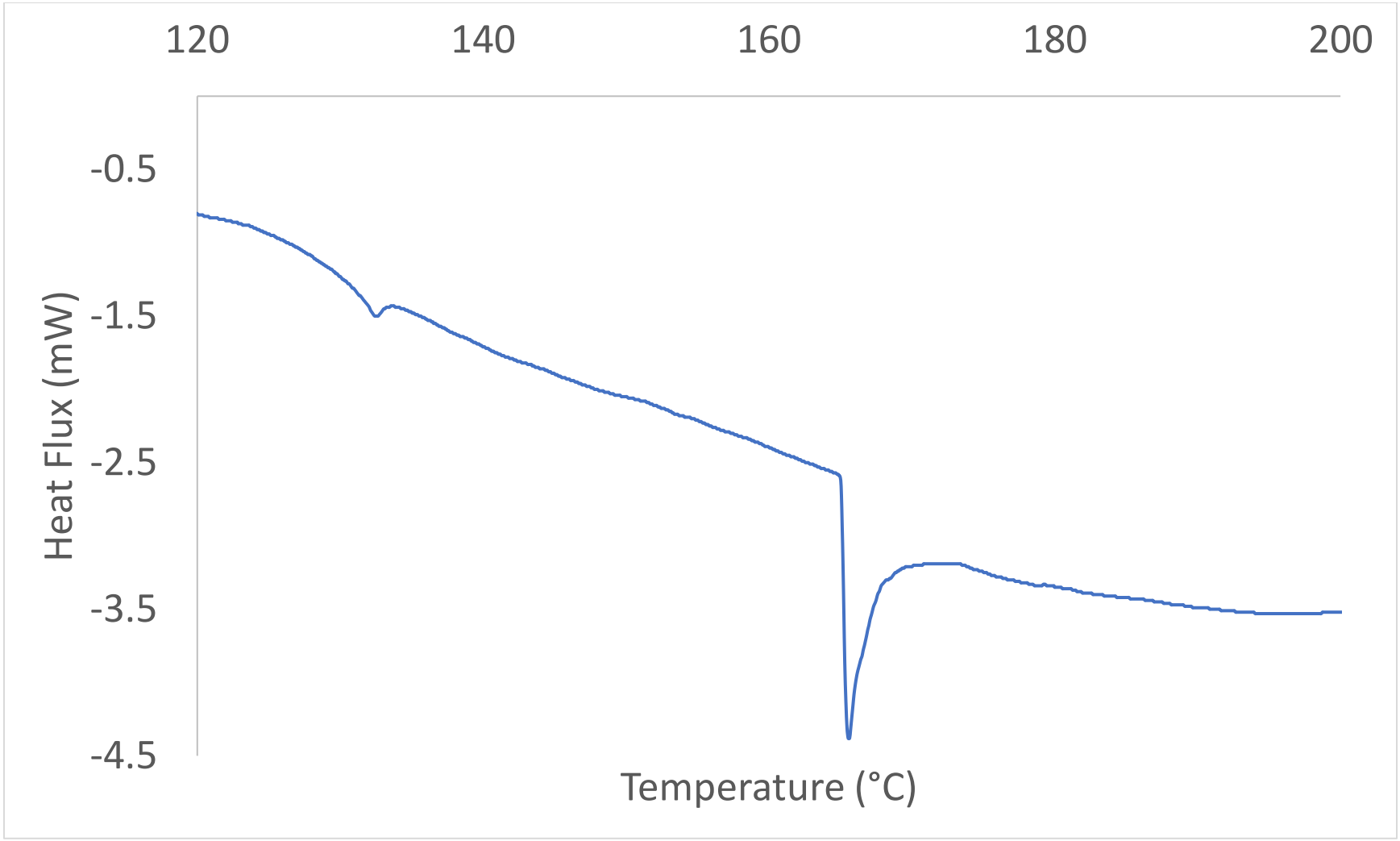

Melting profile of $Na_2[Sb_2\text{-}L(+)\text{-}C_8H_8O_{12}]$ at a ramp rate of 5°C per minute under N_2 atmosphere in aluminum pans.

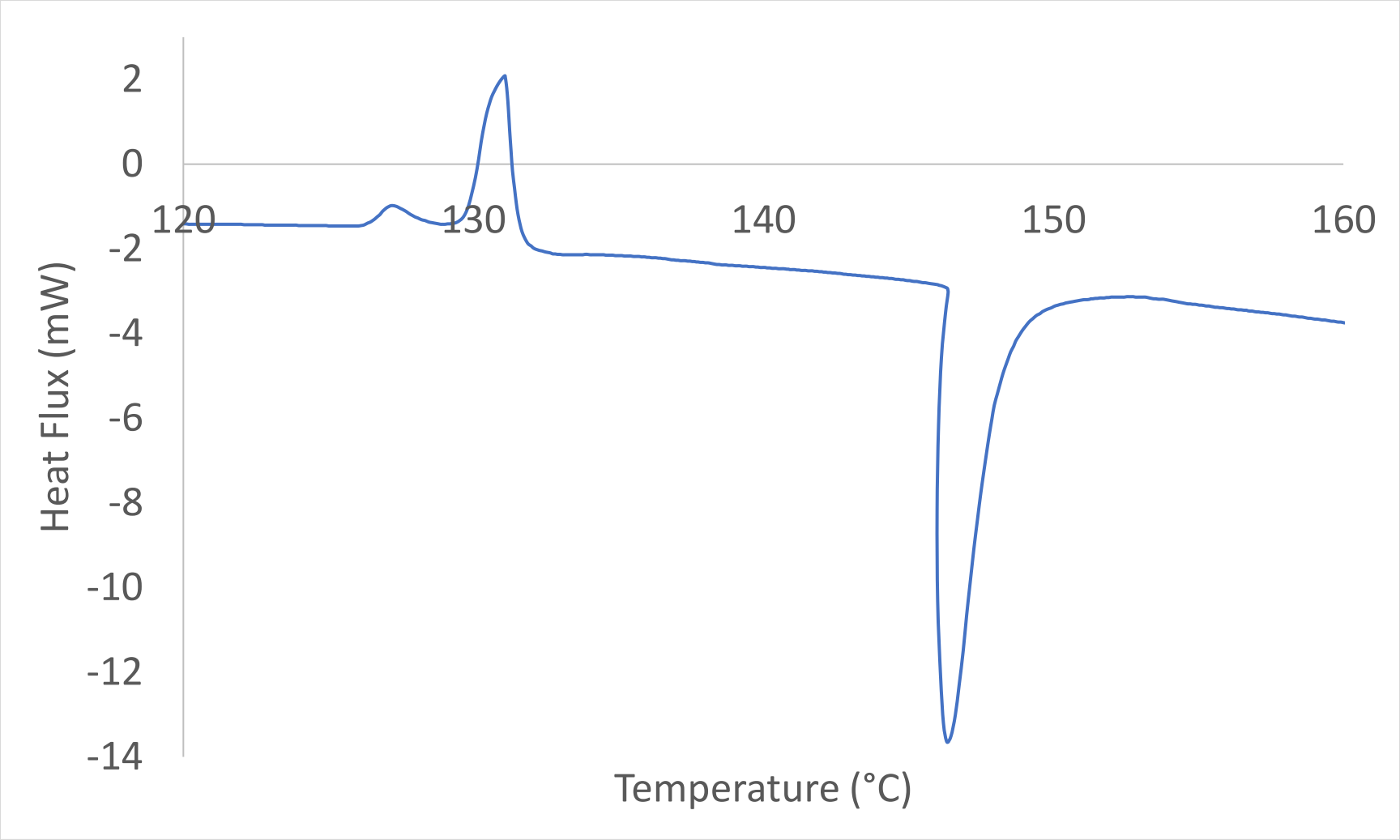

Melting profile of $Na_2[Sb_2\text{-}D(-)\text{-}C_8H_8O_{12}]$ at a ramp rate of 5°C per minute under N_2 atmosphere in aluminum pans.

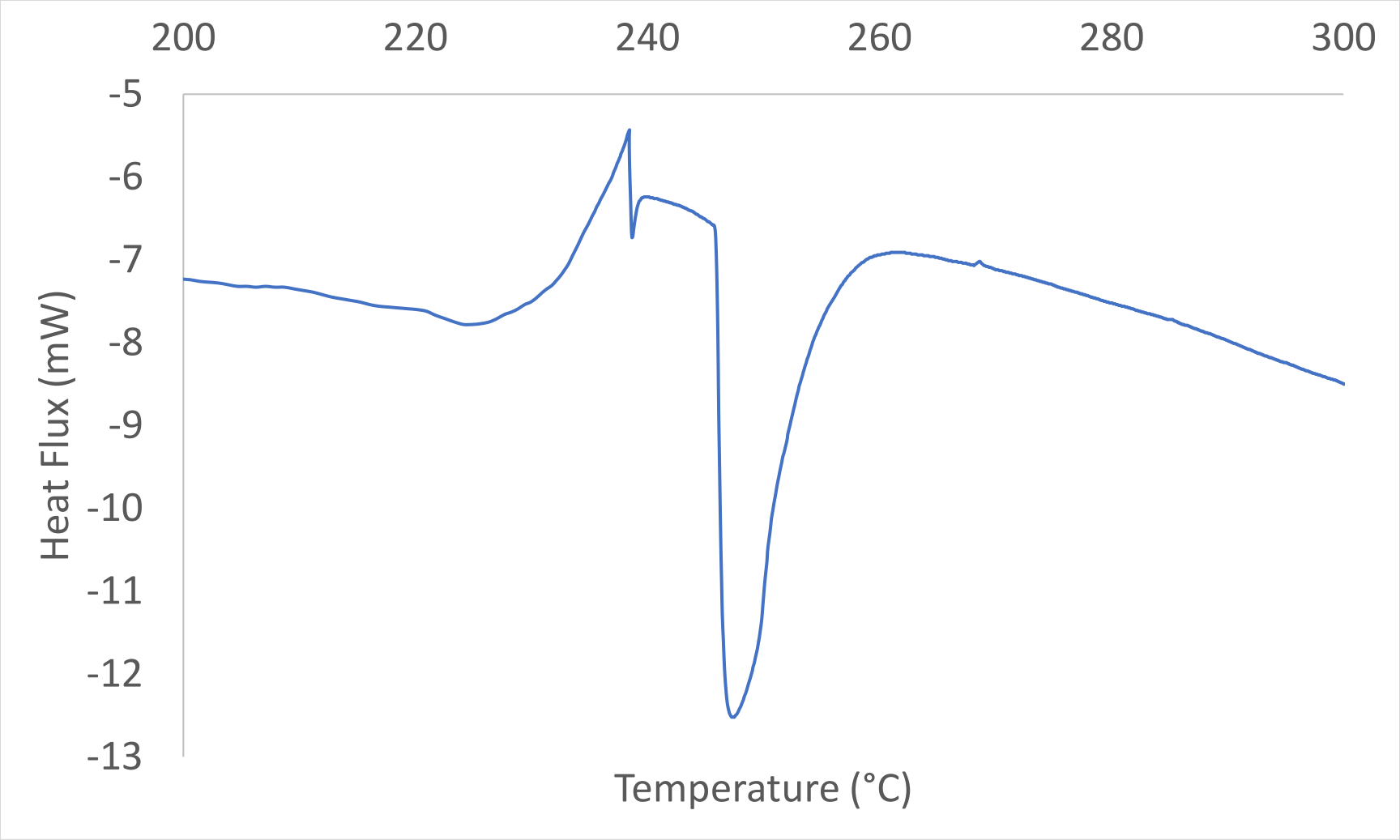

Melting profile of $K_2[Sb_2\text{-}L(+)\text{-}C_8H_8O_{12}]$ at a ramp rate of 5°C per minute under N_2 atmosphere in aluminum pans.

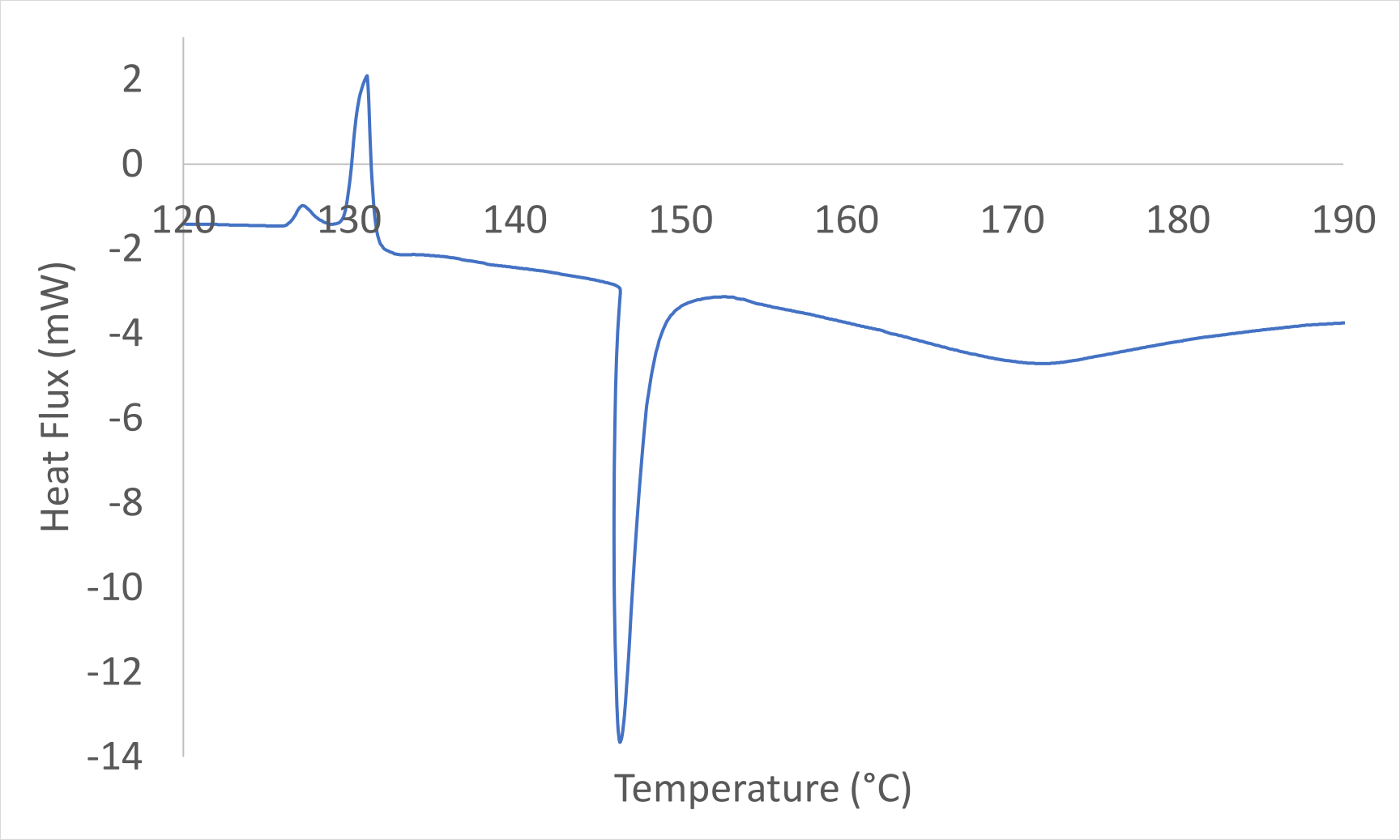

Melting profile of $K_2[Sb_2\text{-}D(-)\text{-}C_8H_8O_{12}]$ at a ramp rate of 5°C per minute under N_2 atmosphere in aluminum pans.

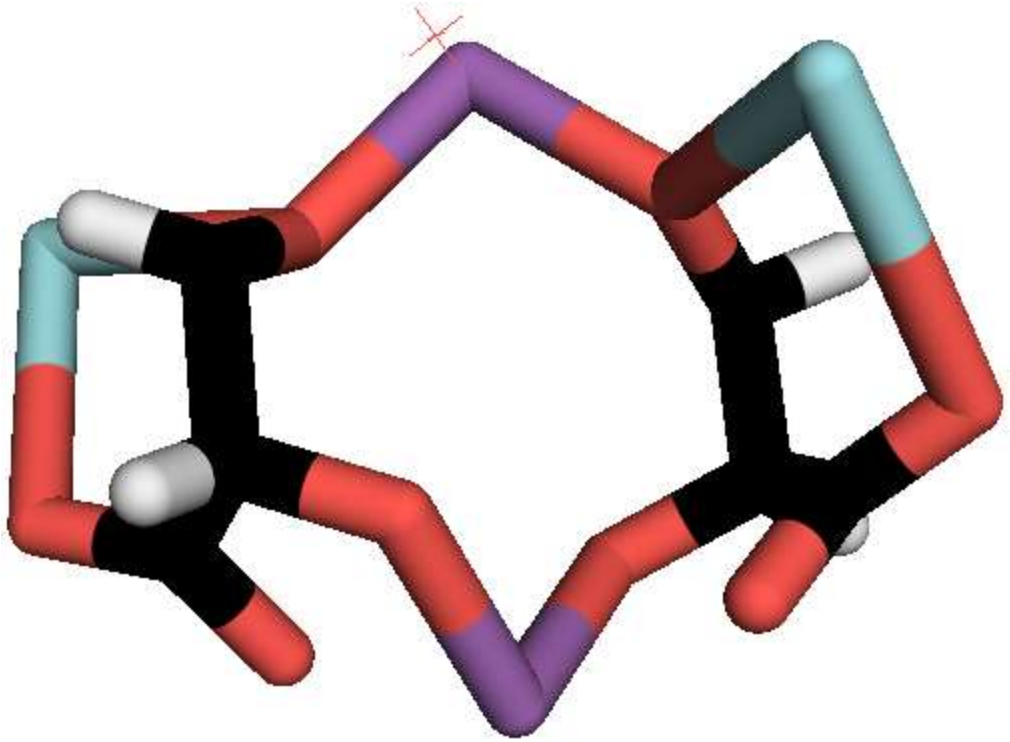

Crystal structure of $K_2[Sb_2\text{-}D(-)\text{-}C_8H_8O_{12}]$ dihydrate, where Sb is purple, K is blue, C is black, H is white, and O is red. Cell: *a* 11.78Å *b* 23.99Å *c* 11.47Å, α 90° β 90° γ 90°

APPENDIX C

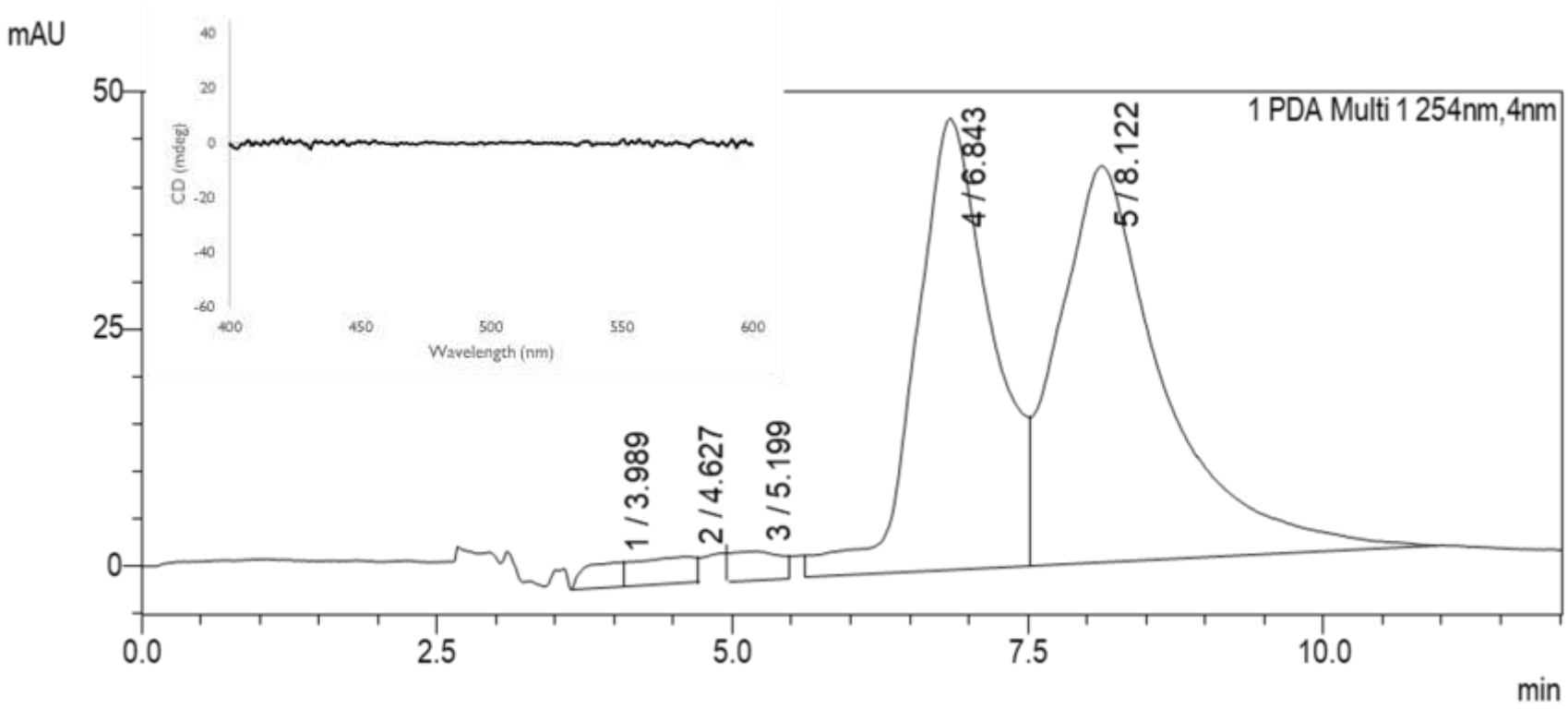

The HPLC profile of [*rac*-Ru(phen)$_2$phendione](PF$_6$)$_2$ using a LARIHC CF6-RN column and CD optical rotation profile of 1 mg·mL^{-1} in reagent grade acetonitrile.

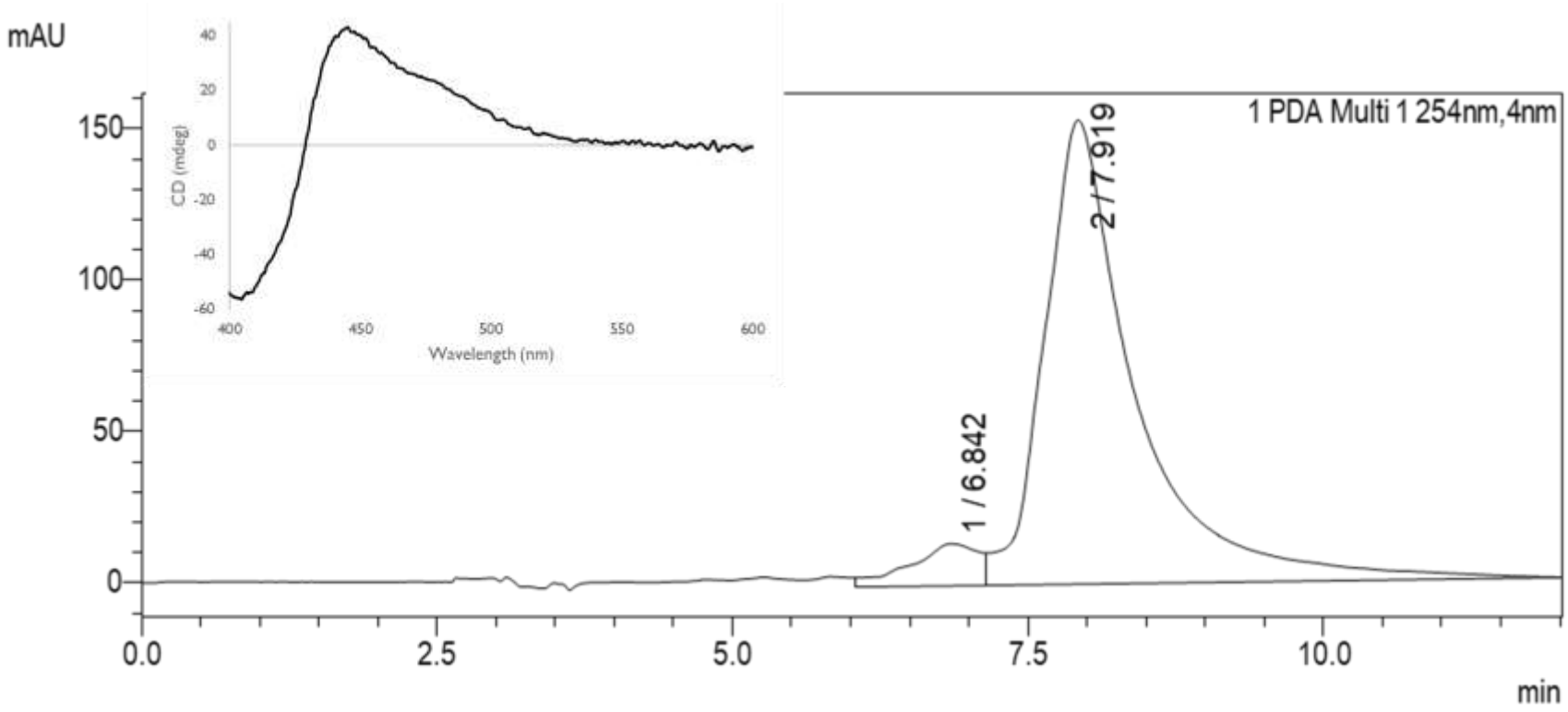

The HPLC profile of $[Ru(phen)_2phendione](PF_6)_2$ that was resolved with $Na_2[As_2(+)tartrate_2]$ and CD optical rotation profile of 1 $mg \cdot mL^{-1}$ in reagent grade acetonitrile.

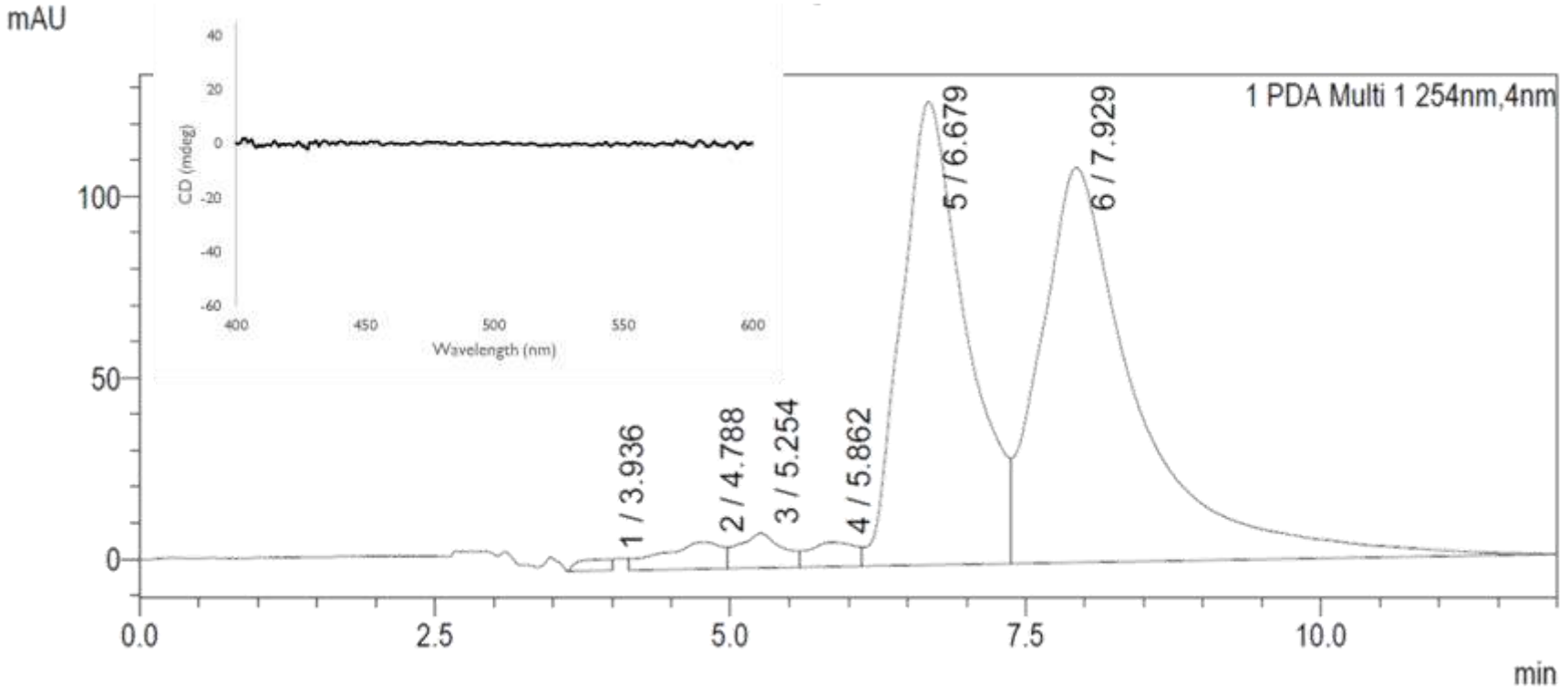

The HPLC profile of $[Ru(phen)_2phendione](PF_6)_2$ that was resolved with $Na_2[Sb_2(+)tartrate_2]$ and CD optical rotation profile of 1 $mg \cdot mL^{-1}$ in reagent grade acetonitrile.

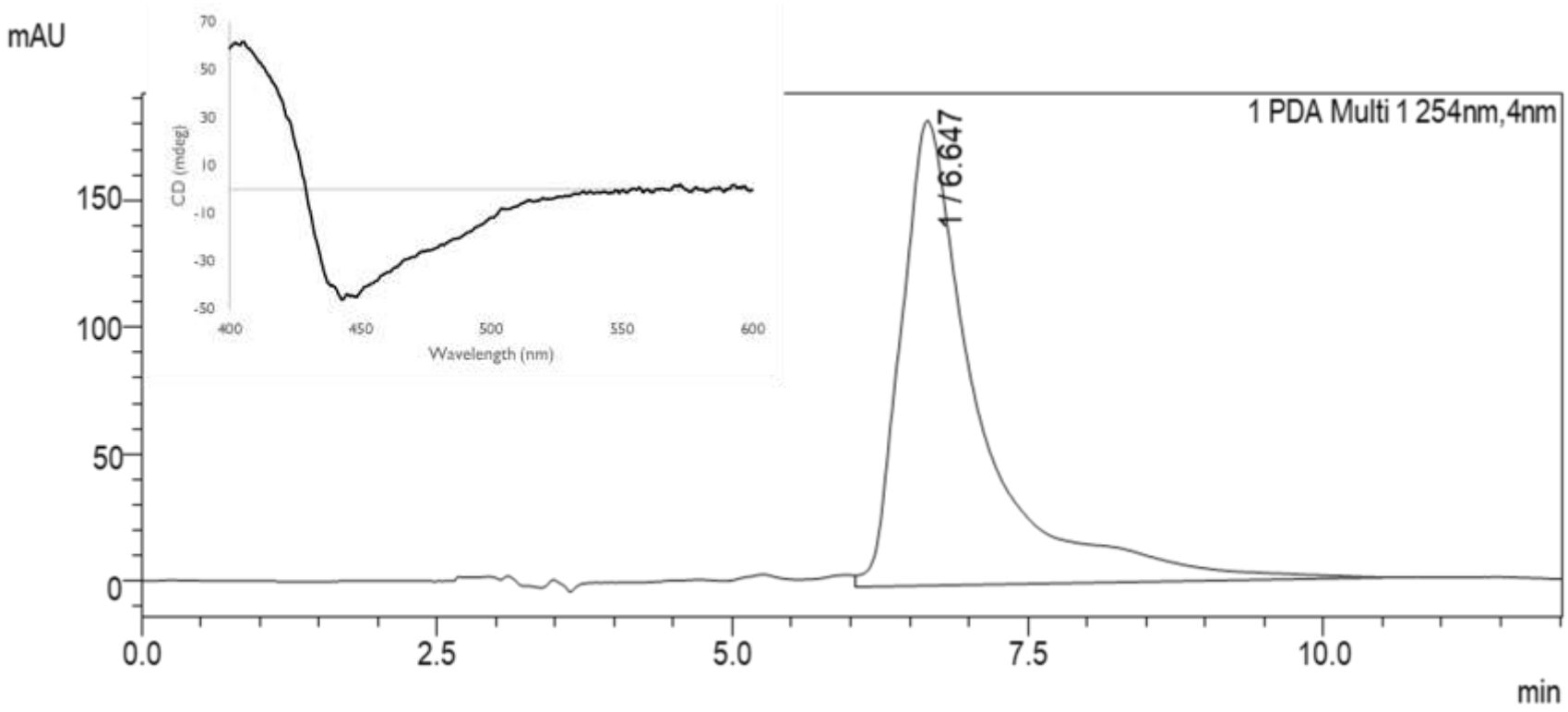

The HPLC profile of $[Ru(phen)_2phendione](PF_6)_2$ that was resolved with $Na_2[As_2(-)tartrate_2]$ and CD optical rotation profile of 1 $mg \cdot mL^{-1}$ in reagent grade acetonitrile.

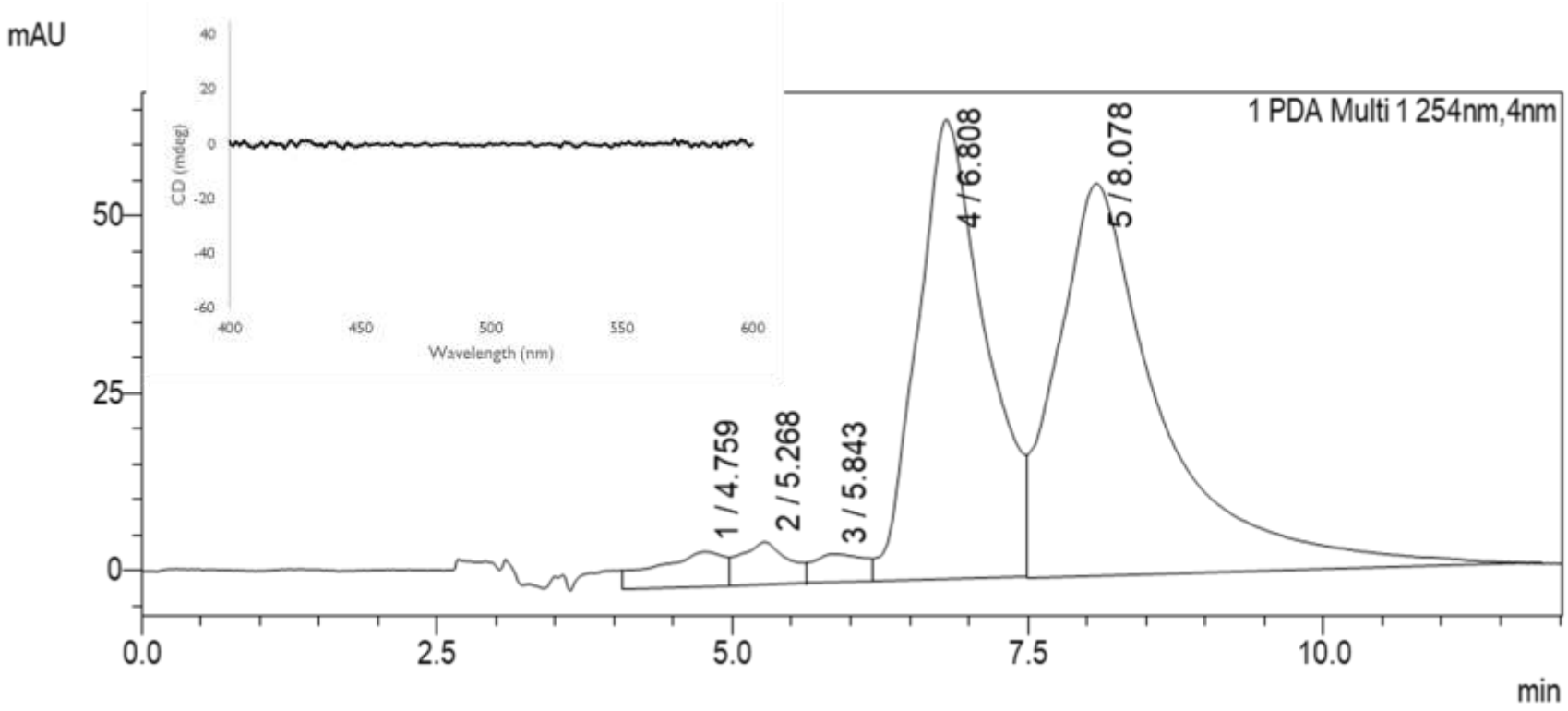

The HPLC profile of $[Ru(phen)_2phendione](PF_6)_2$ that was resolved with $Na_2[Sb_2(-)tartrate_2]$ and CD optical rotation profile of 1 $mg \cdot mL^{-1}$ in reagent grade acetonitrile.

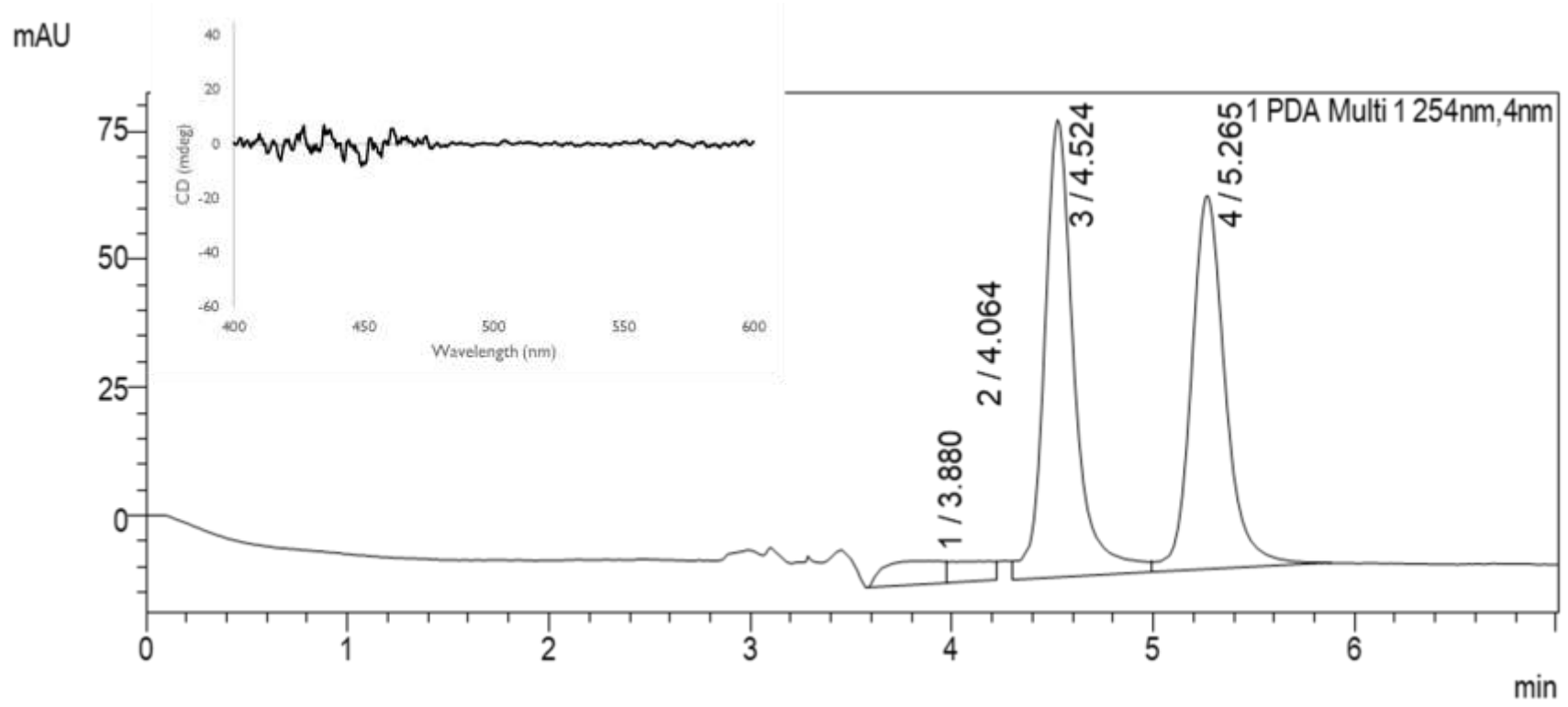

The HPLC profile of [*rac*-Ru(DIP)$_3$](PF$_6$)$_2$ using a LARIHC CF6-RN column and CD optical rotation profile of 1 mg·mL^{-1} in reagent grade acetonitrile.

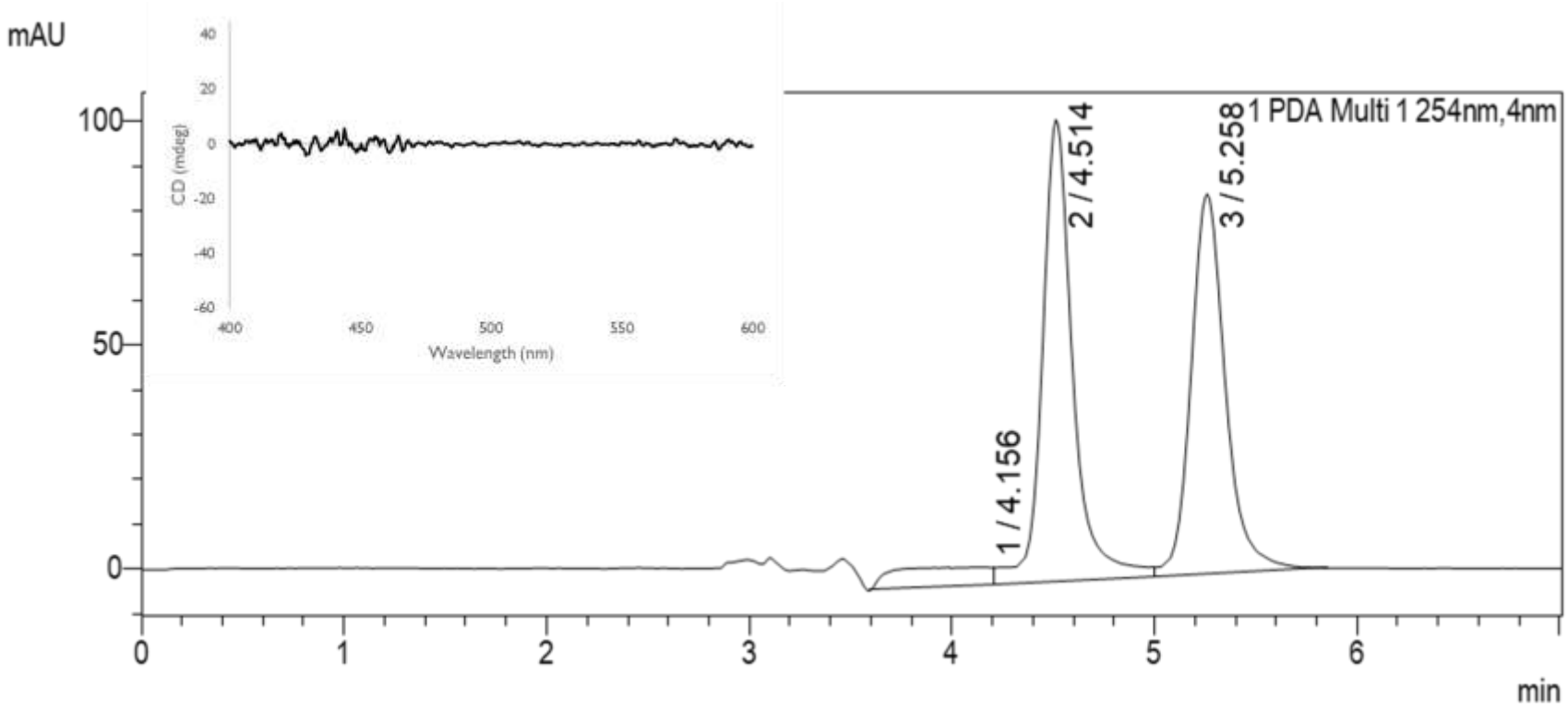

The HPLC profile of $[Ru(DIP)_3](PF_6)_2$ that was resolved with $Na_2[As_2(+)tartrate_2]$ and CD optical rotation profile of 1 $mg \cdot mL^{-1}$ in reagent grade acetonitrile.

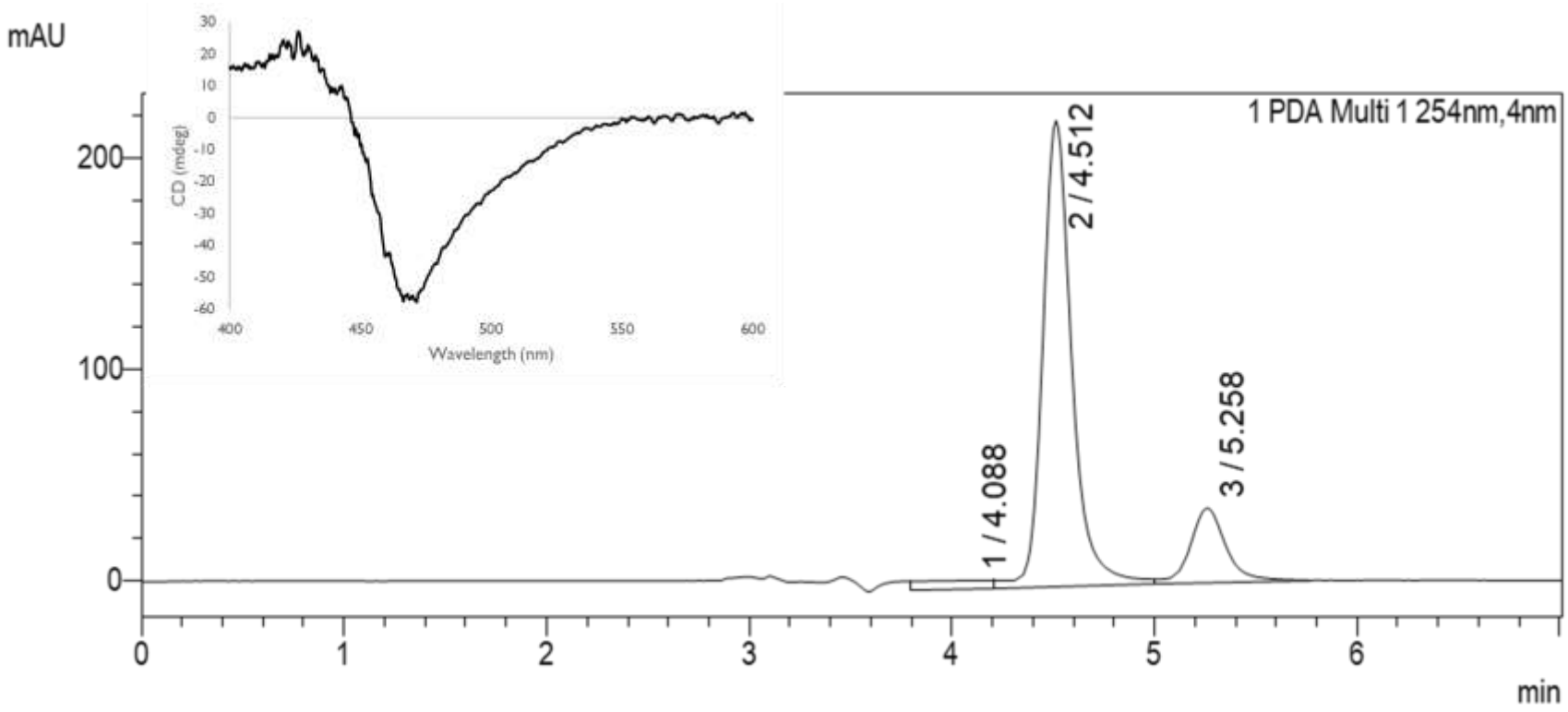

The HPLC profile of $[Ru(DIP)_3](PF_6)_2$ that was resolved with $Na_2[Sb_2(+)tartrate_2]$ and CD optical rotation profile of 1 $mg \cdot mL^{-1}$ in reagent grade acetonitrile.

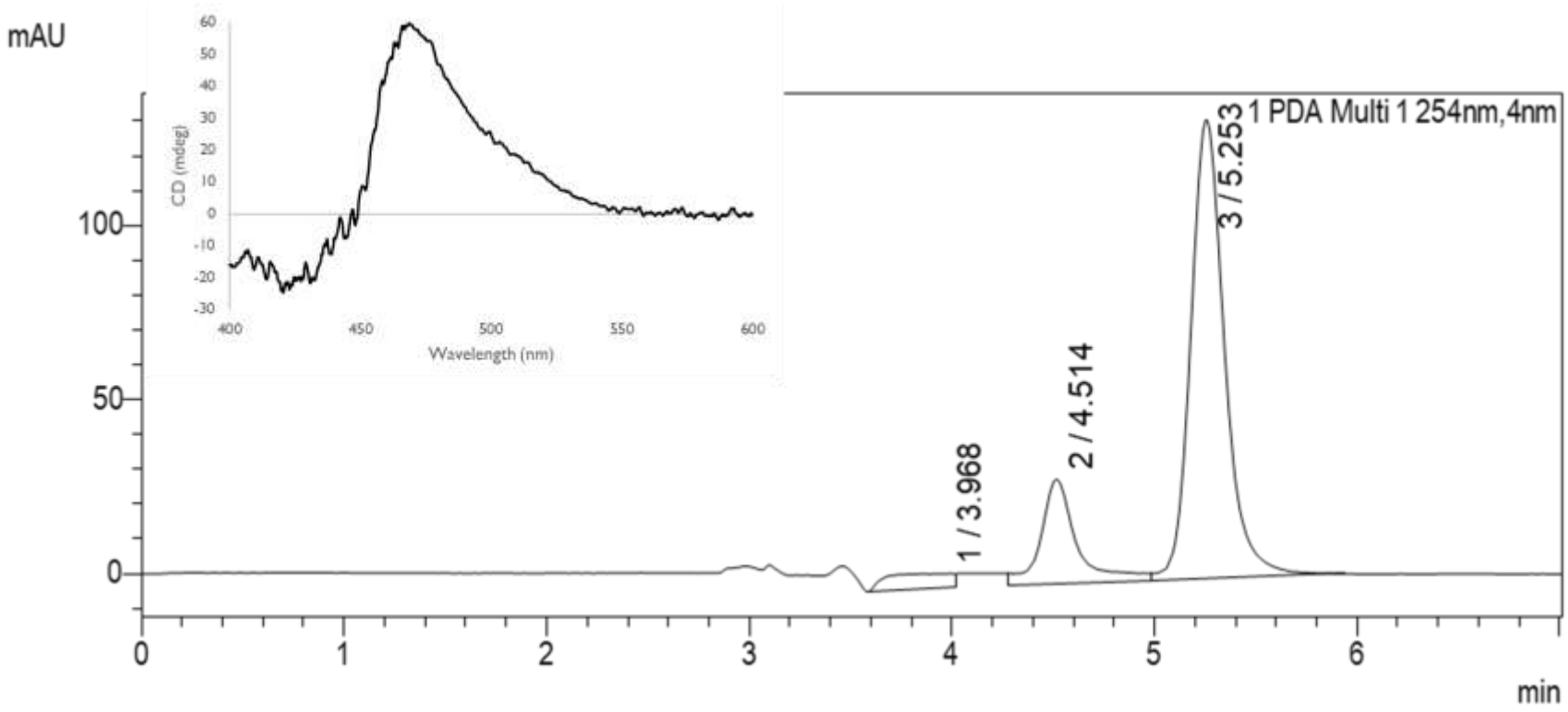

The HPLC profile of $[Ru(DIP)_3](PF_6)_2$ that was resolved with $Na_2[As_2(-)tartrate_2]$ and CD optical rotation profile of 1 $mg \cdot mL^{-1}$ in reagent grade acetonitrile.

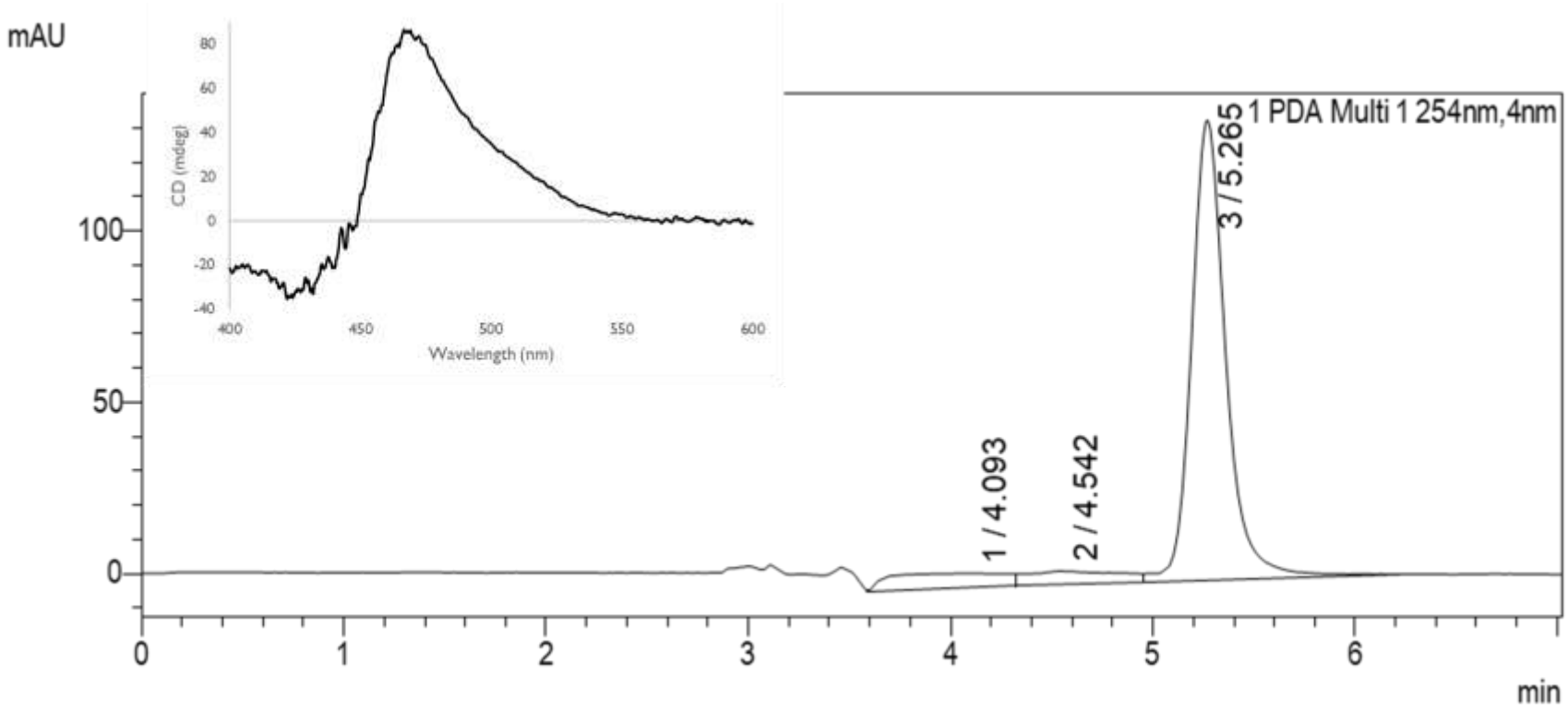

The HPLC profile of $[Ru(DIP)_3](PF_6)_2$ that was resolved with $Na_2[Sb_2(-)tartrate_2]$ and CD optical rotation profile of 1 $mg \cdot mL^{-1}$ in reagent grade acetonitrile.